

Porous Organic Polymers (POPs) in Environmental Remediation

M.Sc. Research Thesis

by

Prince Kumar

Roll No. 2203131024



**DEPARTMENT OF CHEMISTRY
INDIAN INSTITUTE OF TECHNOLOGY
INDORE**

MAY, 2024

Porous Organic Polymers (POPs) in Environmental Remediation

THESIS

*Submitted in partial fulfillment of the
requirements for the award of the degree*

of

Master of Science

by

Prince Kumar

Roll No. 2203131024



**DEPARTMENT OF CHEMISTRY
INDIAN INSTITUTE OF TECHNOLOGY
INDORE**

MAY 2024



INDIAN INSTITUTE OF TECHNOLOGY

CANDIDATE'S DECLARATION

I with this certify that the work being presented in the report entitled **“Porous Organic Polymers (POPs) in Environmental Remediation”** in the partial fulfillment of the requirements for the award of the degree of **MASTER OF SCIENCE** submitted in the **DEPARTMENT OF CHEMISTRY, INDIAN INSTITUTE OF TECHNOLOGY INDORE,** is an authentic record of my work carried out during the period from July 2023 to May 2024 under the supervision of **Prof. Suman Mukhopadhyay,** IIT Indore.

I have not submitted the matter presented in this thesis for the award of any other degree at this or any other institute.

Prince Kumar

Prince Kumar

This is to confirm that the candidate's above statement is accurate to the best of my/ our knowledge.

Prof. Suman Mukhopadhyay

Prince has successfully given his M.Sc. Oral Examination held on **09/05/2024**

Signature of Supervisor of M.Sc. thesis.

Prof. Suman Mukhopadhyay

Convener, DPGC

Dr. Umesh A. Kshirsagar

ABSTRACT

Environmental pollution is increasing alarmingly due to the rapid growth in human civilization and rapid industrialization. Water pollution is one of the types of pollution that need significant attention. Detection of industrial waste and its removal from different wastewater sources is a current challenge. Ionic porous organic polymers (iPOPs) have established themselves as one of the efficient solid-state adsorbents in the remediation of industrial wastewater, but a significant strategy still needs to be developed for designing high-performance iPOP-based solid-state adsorbents. In this report, three cationic porous organic polymers (iPOP-IMZ-1, iPOP-IMZ-2, and iPOP-IMZ-3), considering a guanidium-based cationic building block, have been designed and synthesized. The positive charge density in the polymers was manipulated by changing the secondary building blocks to tune the adsorption ability. The result shows that iPOP-IMZ-2, owing to its higher charge density around the active binding site, has superior adsorption activity compared to the other two polymers. Additionally, due to the fluorescent nature of iPOP-IMZ-2 and iPOP-ZN-3, they were used as fluorescent sensors for the detection of $\text{Cr}_2\text{O}_7^{2-}$ and MnO_4^- ions. Both ions show efficient detection ability at the ppm level.

TABLE OF CONTENTS

CONTENTS	Page No.
LIST OF FIGURES	VIII-X
NOMENCLATURE	XI
ACRONYMS	XII
LIST OF SCHEMES	XIII
Chapter 1: Introduction	1
1.1 General Introduction	2
1.2 Water pollution	2
1.2.1 Chromium-based contamination	2-4
1.2.2 Radioactive contamination	4
1.2.3 Toxic organic dyes	4
1.3 Wastewater Treatment Techniques	5
1.3.1 Sensing of Pollutants	5
1.3.2 Removal of water Pollutants	5
1.3.2.1 Adsorption method	5-6
1.3.2.2 Membrane Filtration	6
1.3.2.3 Chemical Methods	6-7
1.3.2.4 Adsorption method: as an efficient technique	7
1.3.3 POPs: as efficient adsorbent materials	7-8
1.3.4 POPs: as efficient materials for sensing	8
1.4 Porous Organic Polymers (POPs)	8-9
1.4.1 Design and synthesis of building blocks	9

1.4.2 Classification of porous organic polymers (POPs)	9-10
1.4.2.1 Covalent triazine frameworks (CTFs)	10
1.4.2.2 Covalent organic frameworks (COFs)	10-11
1.4.2.3 Hypercrosslinked polymers (HCPs)	11
1.4.2.4 Conjugate microporous polymers (CMPs)	11-12
1.4.3 Classification of POPs on the basis of charge	12
1.4.3.1 Neutral porous organic polymers	12-13
1.4.3.2 Ionic porous organic polymers (iPOPs)	13-14
1.5 Characterization of POPs	14
1.5.1 Fourier-transform infrared spectroscopy (FT-IR)	14-15
1.5.2 Solid-state NMR	15
1.5.3 TGA (Thermogravimetric analysis)	15
1.5.4 BET	15-16
1.5.5 PXRD	16
1.5.6 FESEM	16
1.6 Organization of the Thesis	17
Chapter 2: Literature Survey and Project Motivation	18
2.1 Review of Past Work and Project Motivation	19-22
Chapter 3: Experimental Section	23
3.1 Reagent & Chemicals	24
3.2 Instrumentation and Methods	24
3.3 Synthesis of the monomers	24

3.3.1 Synthesis of triaminoguanidinium nitrate	24-25
3.3.2 Synthesis of 4-imidazolyl-benzaldehyde	25
3.3.3 Synthesis of GID.HNO_3	25
3.3.4 Synthesis of 2,4,6-tris(-(bromomethyl) phenyl) -1,3,5-triazine (TTBr)	25-26
3.4 Synthesis of ionic porous organic polymers	26
3.5 Adsorption Study	26
3.5.1 Procedures of time-dependent study of anionic contamination adsorption from aqueous solution using synthesized iPOPs	26-27
3.5.2 Calculation of adsorption capacity of iPOPs Towards oxo-anions and anionic dyes.	27-28
3.6 Sensing Study	28
3.6.1 Fluorescence sensing $\text{Cr}_2\text{O}_7^{2-}$ and MnO_4^- by using iPOPs	28
Chapter 4: Results and Discussion	29
4.1 Structure and Synthesis	30
4.2 Reaction Schemes	30-34
4.3 Characterization	35
4.3.1 Characterization of starting material of pops	35-38
4.3.2 Characterization of iPOPs	38-44
4.4 Analysis of adsorption of metal-based oxo-anions by iPOPs	44-46
4.5 Analysis of adsorption of anionic dyes by iPOPs	46-50

4.6 Fluorescence sensing	51-53
Chapter 5: Conclusion and Future Scope	55
5.1 Conclusion	56
5.2 Future Scope	56
References	57-68

LIST OF FIGURES

Figure No.	Description	Page No.
Figure 1.1	Source, cause, and effects of Cr-based Contamination.	3
Figure 1.2	General mechanism of adsorption methods.	6
Figure 1.3	Pictorial diagram of porous organic polymer.	9
Figure 1.4	Structure of covalent triazine framework.	10
Figure 1.5	Structure of hypercrosslinked polymers.	11
Figure 1.6	Structure of covalent microporous polymer.	12
Figure 1.7	Synthetic diagram of a neutral porous organic polymer.	13
Figure 1.8	Structure of cationic, anionic, and Zwitterionic porous organic polymer.	14
Figure 2.1	General linkages used in porous organic polymers.	19
Figure 2.2	Known examples of building blocks/groups used in cationic porous organic polymers.	20
Figure 2.3	The structure of the different types of monomers used to make the polymers used in this work.	22
Figure 4.1	^1H NMR of triaminoguanidinium nitrate.	35
Figure 4.2	^{13}C NMR of triaminoguanidinium nitrate.	35
Figure 4.3	^1H NMR 4-imidazolyl-benzaldehyde.	36
Figure 4.4	^{13}C NMR of 4-imidazolyl-benzaldehyde.	36
Figure 4.5	^1H NMR of GID.HNO_3 .	37
Figure 4.6	^1H NMR of 2,4,6-tris (-(bromomethyl) phenyl)-1,3,5-triazine.	38

Figure 4.7	^{13}C NMR of 2,4,6-tris (-(bromomethyl) phenyl)-1,3,5-triazine.	38
Figure 4.8	FTIR Spectra of (a) iPOP-IMZ-1 (b) iPOP-IMZ-2 (c) iPOP-IMZ-3.	39
Figure 4.9	^{13}C CP/MAS NMR for (a) iPOP-IMZ-1, (b) iPOP-IMZ-2 (c) iPOP-IMZ-3.	40
Figure 4.10	TGA curve of iPOP-IMZ-1, iPOP-IMZ-2 and iPOP-IMZ-3.	40
Figure 4.11	(a) N_2 adsorption isotherm and (b) Pore size distribution on curve of iPOP-IMZ-1, iPOP-IMZ-2, and iPOP-IMZ-3 respectively.	41
Figure 4.12	The PXRD pattern of (a) iPOP-IMZ-1, (b) iPOP-IMZ-2 and (c) iPOP-IMZ-3.	41
Figure 4.13	FE-SEM image of (a) iPOP-IMZ-1, (b) iPOP-IMZ-2, (c) iPOP-IMZ-3.	42
Figure 4.14	The EDX analysis of iPOP-IMZ-1	42
Figure 4.15	The EDX analysis of iPOP-IMZ-2	43
Figure 4.16	The EDX analysis of iPOP-IMZ-3	43
Figure 4.17	Mapping analysis of the iPOP-IMZ-1	43
Figure 4.18	Mapping analysis of the iPOP-IMZ-2	44
Figure 4.19	Mapping analysis of the iPOP-IMZ-3	44
Figure 4.20	The UV-vis spectra, at different times for aqueous solution of $\text{Cr}_2\text{O}_7^{2-}$ in the presence of (a) iPOP-IMZ-1, (b) iPOP-IMZ-2, (c) iPOP-IMZ-3. (d) Decrease in the concentration and (e) removal (%), with time in the presence of iPOPs (f) The pseudo-second-order kinetics of the aqueous solution of $\text{Cr}_2\text{O}_7^{2-}$.	45
Figure 4.21	The UV-vis spectra, at different times for aqueous solution of MnO_4^- in the presence of (a) iPOP-IMZ-1, (b) iPOP-IMZ-2, (c) iPOP-IMZ-3. (d) Decrease in the concentration and (e) removal (%), with time in the presence of iPOPs (f) The pseudo-second-order kinetics of the aqueous solution of MnO_4^- .	46

- Figure 4.22** The UV-vis spectra, at different times for aqueous solution of Methyl Orange (MO) in the presence of (a) iPOP-IMZ-1, (b) iPOP-IMZ-2, (c) iPOP-IMZ-3. (d) Decrease in the concentration and (e) removal (%), with time in the presence of iPOPs (f) The pseudo-second-order kinetics of the aqueous solution of Methyl Orange (MO). 47
- Figure 4.23** The UV-vis spectra, at different times for aqueous solution of Amaranth in the presence of (a) iPOP-IMZ-1, (b) iPOP-IMZ-2, (c) iPOP-IMZ-3. (d) Decrease in the concentration and (e) removal (%), with time in the presence of iPOPs (f) The pseudo-second-order kinetics of the aqueous solution of Amaranth. 48
- Figure 4.24** Langmuir isotherm of $\text{Cr}_2\text{O}_7^{2-}$ (24a- 24c) and MnO_4^- (24d-24f) in the presence of iPOP-IMZ-1, iPOP-IMZ-2, and iPOP-IMZ-3 respectively. 49
- Figure 4.25** Langmuir isotherm of MO (25a- 25c) and Amaranth (25d-25f) in the presence of iPOP-IMZ-1, iPOP-IMZ-2, and iPOP-IMZ-3 respectively. 49
- Figure 4.26** Diminish the color of (a) $\text{Cr}_2\text{O}_7^{2-}$, (b) MnO_4^- , (c) MO, and (d) Amaranth in the presence of iPOPs respectively. 50
- Figure 4.27** Relative % removal at different pH of (a) $\text{Cr}_2\text{O}_7^{2-}$, (b) MnO_4^- , (c) MO, and (d) Amaranth in the presence of iPOPs respectively. 50
- Figure 4.28** In the presence of $\text{Cr}_2\text{O}_7^{2-}$, (a) fluorescence spectra (b) Stern–Volmer equation fitting. In the presence of permagnent ions, (c) fluorescence spectra and (d) Stern–Volmer equation fitting of iPOP-IMZ-2. 52
- Figure 4.29** In the presence of dichromate ions, (a) fluorescence spectra (b) Stern–Volmer equation fitting. In the presence of permanent ions, (c) fluorescence spectra and (d) Stern–Volmer equation fitting of iPOP-IMZ-3. 53
- Figure 4.30** Fluorescence quenching of (a) iPOP-IMZ-2 and (b) iPOP-IMZ-3 in the presence of other anions. 53

NOMENCLATURE

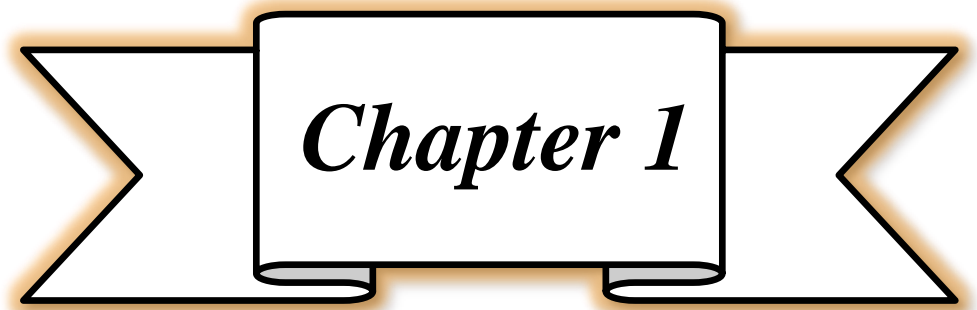
°C	Degree Centigrade
g	Gram
mg	Milligram
mL	Millilitre
mmol	Millimole
μL	Microlitres
mM	Milli Molar
M	Molar
mol	Mole
nm	Nanometres
%	Percentage
s	Seconds
cm	Centimetre

ACRONYMS

C	Carbon
DMSO	Dimethyl Sulphoxide
DMF	Dimethyl formamide
H	Hydrogen
MeOH	Methanol
N	Nitrogen
NMR	Nuclear Magnetic Resonance
FT-IR	Fourier Transform-Infrared
PXRD	Powder X-Ray Diffraction
FE-SEM	Field Emission Scanning Electron Microscope
H₂O	Water
BET	Brunauer-Emmett-Teller
UV	Ultraviolet
TBrMB	1,3,5-trisbromomethylbenzene
DBrXy	α,α' -dibromo-p-xylene
MO	Methyl Orange

LIST OF SCHEMES

Scheme No.	Description	Page No.
Scheme 4.1	Synthesis of triaminoguanidinium nitrate	30
Scheme 4.2	Synthesis of 4-imidazolyl-benzaldehyde	30
Scheme 4.3	Synthesis of GID.HNO ₃	31
Scheme 4.4	Synthesis of 2,4,6-tris (-(bromomethyl) phenyl)- 1,3,5-triazine (TTBr)	31
Scheme 4.5	Synthesis of iPOP-IMZ-1	32
Scheme 4.6	Synthesis of iPOP-IMZ-2	33
Scheme 4.7	Synthesis of iPOP-IMZ-3	34



Introduction

1.1 General introduction

In the current era, the unchecked rise in industrial activity in various parts of the world has triggered various environmental consequences that are difficult to ignore. From increased air and water pollution to deforestation, the impact of industrialization on the environment is far-reaching and alarming. At this time, no part of the Earth is left untouched by environmental pollution, and its effect can be felt from the ocean depths to various atmospheric layers. The effects of this phenomenon have far-reaching consequences for our planet, impacting the delicate balance of our environment¹, aquatic and wildlife^{2,3}, climate, and biodiversity. These consequences, in turn, have an impact on humanity and other life forms on Earth in various ways⁴.

1.2 Water pollution

The continuous growth of the Earth's population is putting pressure on water resources. That means oceans, rivers, lakes, and other water resources are being exploited by human activity, which reduces the quality of Earth's surface water. Water pollution can be defined as the presence of one or more substances in water that have accumulated to such an extent that they cause harm to animals or humans. The major sources of such contaminants are mainly the industries that release gallons of untreated water to several water sources, significantly increasing water pollution. Among various active water pollutants, inorganic oxo-anions^{7,8} and organic dyes^{8,9} are some active species that have significant ill effects on human health.

1.2.1 Chromium-based contamination

Chromium (Cr) is the most abundant element found in the Earth's crust¹⁰. It is widely used in various applications such as tanning, electroplating, steel production, alloying, wood preservation, pigmentation, textile dyeing, nuclear reactors, and preparation of ceramic glazes. The uncontrolled

release of Cr-containing effluents into the environment causes significant Cr contamination¹¹⁻¹³. The highly toxic Cr (VI) form is very soluble and mobile, causing devastating impacts on animals and humans. Researchers have reported that the inhalation of hexavalent chromium (Cr (VI)) can cause lung cancer in human and animal bodies through long-term exposure¹⁴. At the same time, hexavalent chromium deposited on the fish's gill exerts lethal effects on the liver and kidney, even at moderate levels^{15,16}.

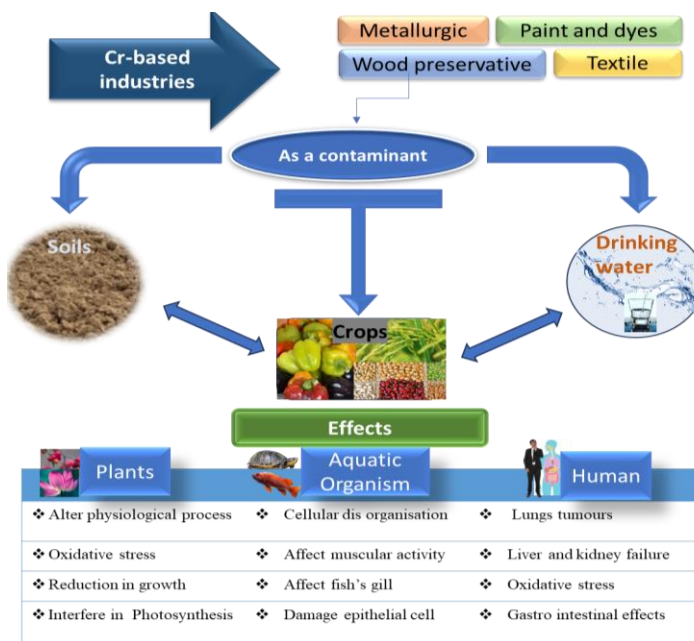


Figure 1.1 Source, cause, and effects of Cr-based contamination.

Many studies have reported that Cr (VI) also has adverse effects on plants. Delayed seed germination, decrease in photosynthetic rate, and inhibition in enzymatic activities are some of the common examples that ultimately affect flowering rate, fruit yields, and the quality of plants¹⁷.

Cr-based contamination in wastewater is considered the most persistent pollutant, according to the U.S. Environmental Protection Agency (US EPA). Considering the adverse effects of Cr(VI) on humans, aquatic, and wildlife, it is a global concern to detect and remediate Cr(VI) based pollutants¹⁸.

1.2.2 Radioactive contamination

A β -emitter with a long half-life of 2.13×10^5 years, technetium-99 (^{99}Tc) is the most problematic radionuclide. It is produced annually with 21 kg with a high fission yield of 6 % by a 1 GWe-scale nuclear reactor. TcO_4^- is one of the most prominent forms of ^{99}Tc -containing various forms in atomic fuel and environments under toxic conditions. It has a highly mobile nature, high water solubility, and remarkable environmental stability¹⁹. TcO_4^- has been used extensively in weapon testing, nuclear fuel repossessing, and other nuclear accidents, and discharged from these applications have contributed significantly to environmental contamination. It shows various adverse effects on the human body, plant tissues, and aquatic organisms due to β -emitter radioactive nature^{20,21}.

1.2.3 Toxic organic dyes

Various compounds have been used in the textile industry to colorate garments, but synthetic dyes have been used at the most prominent level²². Among various dyes used at industrial levels, azo bond ($-\text{N}=\text{N}-$) containing organic dyes appeared to be the most common [toxic compound]. These dyes are very harmful, carcinogenic, and mutagenic, which cause severe health-related problems such as damage to nervous systems and liver and brain functioning. If consumed, it could cause allergic reactions, endocrine disruptions, and even tumor formation in some cases. At the same time, regular inhalation of such chemicals might cause asthma, eye irritation, wheezing, and breathing problems. Since these dyes are not biodegradable, they harm the environment, wildlife, and aquatic life^{23,24}.

1.3 Wastewater Treatment Techniques

For achieving efficient water purification technology, the detection of the pollutants and their effective separation are important²⁵.

1.3.1 Sensing of pollutants

The detection of the presence of heavy metal-based contamination in wastewater is equally important as its removal. Developing technologies to detect heavy-metal-based pollutants from wastewater is one of the current interests in the scientific community. Various traditional techniques have been developed in the last decade for detecting heavy metal-based pollutants in wastewater, like ion chromatography, surface-enhanced Raman scattering method, metal detectors, etc. These techniques have many disadvantages, such as high cost, complicated instrument handling, time consumption, etc., making them non-facile. Sensing the pollutants based on luminescence properties has excellent benefits. Its cheaper cost and simple operation make it a facile technique compared to traditional methods²⁶⁻²⁸.

1.3.2 Removal of water pollutants

Removing toxic pollutants from wastewater is another current scientific concern worldwide. Several techniques have been developed in the recent past, *viz.* chemical and bio precipitation, electro and photocatalytic degradation of the pollutants, adsorption, etc²⁹.

1.3.2.1 Adsorption method

Adsorption phenomena are surface phenomena that involve the adhesion of adsorbate (molecules or particles from fluids such as liquid or gas) in higher concentrations on the surface of adsorbent (solid or liquid) substances. In the adsorption process, three main steps include:

1. The adsorbate migrates to the outer shell of the adsorbent.
2. Undergoes intraparticle diffusion into the pores of the adsorbent.
3. The solute is adsorbed and desorbed.

Characteristics of the adsorbate, adsorbent, and matrix play a crucial role in controlling the rate of all subsequent steps generally occurring in the adsorption process. Typically, this technique follows two phenomena, physisorption and chemisorption. In the physisorption phenomenon, physical interactions occur between the adsorbed molecules and the adsorbent materials due to weak forces of interactions, such as the van der Waals force, which makes it a reversible process. Chemical bonding forms between adsorbed molecules and adsorbent materials in the chemisorption phenomenon³⁰.

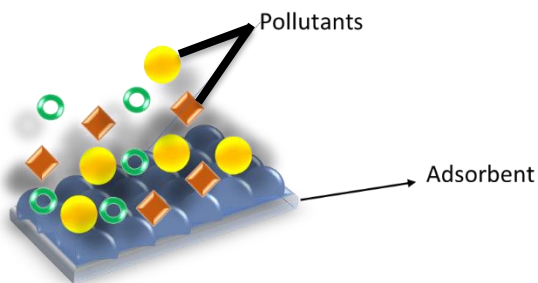


Figure 1.2 General mechanism of adsorption methods.

1.3.2.2 Membrane Filtration

Membrane filtration is also one of the common techniques in wastewater treatment. Hydrophilicity and surface charge of the membrane in this technique can play a crucial role in determining its rejection, permeability, and antifouling performance³¹.

1.3.2.3 Chemical methods

Among various chemical methods for wastewater remediation, oxidation is one of the widely used methods, including photochemical oxidation, electrochemical oxidation, photo-electrochemical oxidation, etc. All these oxidation processes are based on the reactive oxygen species generation principle (Scicardi 2020). However, these techniques have established

themselves as efficient techniques; most of the methods commonly use novel metal-based catalysts. At the same time, high energy requirements in these processes make them inefficient to be used at the industrial level^{32,33}.

1.3.2.4 Adsorption method: as an efficient technique

Apart from several advantages, the techniques mentioned above also suffer significant disadvantages. Chemical methods are easy to handle, but they are not feasible from an economic perspective. The membrane filtration method is also not cost-effective due to its high energy requirement, significant maintenance, and operational cost. On the other hand, the adsorption method in wastewater remediation is a widely recognized, well-developed, significantly economical, and reliable method (Liu et al. 2020). According to the United States Environmental Protection Agency (USEPA), the adsorption process is the most prescient method compared to other conventional treatment processes for wastewater treatment processes (Anil et al.2020). Its flexibility, simplicity, and economic feasibility make it more prominent than other techniques. In this technique, contaminants bind to the external and internal surfaces of solid materials called adsorbent materials^{35,36}.

1.3.3 POPs: as efficient adsorbent materials

In the process of developing efficient porous material-based adsorbents for wastewater remediation, several novel materials have been tried in the recent past, like zeolites, ionic metal-organic framework (MOF), ionic hydrogels and aerogels, ion exchange resins, etc. There are several shortcomings of these materials, such as low acid and base tolerance, poor stability in harsh conditions, low surface area, low reusability, poor pollutant capture ability, and dual activity to be used in capturing used against pollutants present in water and air, which restrict their practical use. In this regard, ionic porous polymers (iPOPs) have emerged as a new type of porous material that is getting popular in scavenging ionic pollutants in

recent times. Their stable organic skeleton, high stability in harsh conditions, high surface area, exchangeable counter ions, and reusability make them ideal to be used in wastewater remediation^{37,38}.

1.3.4 POPs: as efficient materials for sensing

POPs also play a crucial role in the sensing of metal-based pollutants. Owing to a large accumulation of conjugated organic building blocks, sometimes POPs show fluorescent properties. The fluorescent nature of the POPs can be utilized in the detection of several foreign chemicals present in water following an optical (luminescence) sensing technique. In the series of developments of POP-based sensors, ionic porous organic polymers (iPOP) could be a promising candidate. Due to particular charged sites, iPOPs could effectively provide binding sites to the foreign elements that help the sensing mechanism. The main reason for the fluorescent properties in some polymers is the $\pi \rightarrow \pi^*$ transition in the organic building blocks and π electron cloud stacking in the polymers. The accumulation of host ions in the charged polymeric skeleton in iPOPs might hamper the $\pi \rightarrow \pi^*$ transition in the polymeric network; at the same time, their presence in the polymeric layers interferes with interlayer stacking, causing the quenching of the fluorescent properties of the polymers³⁹⁻⁴¹.

1.4 Porous Organic Polymers (POPs)

Porous organic polymers are a sub-class of porous materials that combine with properties like high surface area, tuneable porosity, and stability even in harsh conditions. These are synthesized by combinations of organic building blocks through strong covalent bonds. The building blocks mainly contain light elements like C, N, O, B, S, etc., to ensure permanent porosity and light density; based on the choice of organic building blocks, POPs are utilized in various applications⁴².

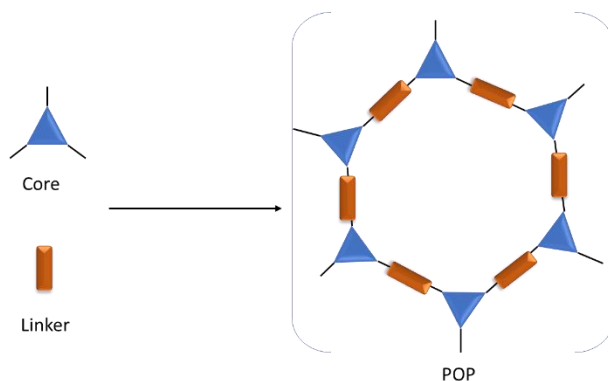


Figure 1.3 Pictorial diagram of porous organic polymer

1.4.1 Design and synthesis of building blocks

While designing the organic building blocks for POP synthesis, some things are kept in mind, such as (1) the presence of aromatic rings that provide conjugated systems and (2) the presence of some rigid linker that helps to control the porosity and surface area of POPs (3) the presence of some different core groups (2 D and 3 D) which help to architect topological networks and (4) the presence of crosslinking sites that allow for the synthesis of polymeric networks. The porous organic polymer is constructed by the composition of organic building blocks through various linkages like imine, azine, -C-C-, hydrazine, baronet ester, triazine, and diazine ring formation, etc⁴³.

1.4.2 Classification of porous organic polymers (POPs)

Based on the structural diversity, porous organic polymers can be classified into various subclasses such as covalent triazine frameworks (CTFs), covalent organic frameworks (COFs), hypercrosslinked polymers (HCPs), conjugated microporous polymers (CMPs), etc⁴⁴.

1.4.2.1 Covalent triazine frameworks (CTFs)

Covalent triazine frameworks (CTFs) are also one subclass of porous organic polymers that contain a triazine ring as a core building

block45. The CTFs were synthesized through superacid-catalyzed trimerization, Yamamoto coupling, Suzuki cross-coupling, etc., with mostly conjugate and layered structure monomers. It shows various applications in various fields like water splitting, CO₂ reduction, pollutant degradation, semiconductor devices, etc^{45,46}.

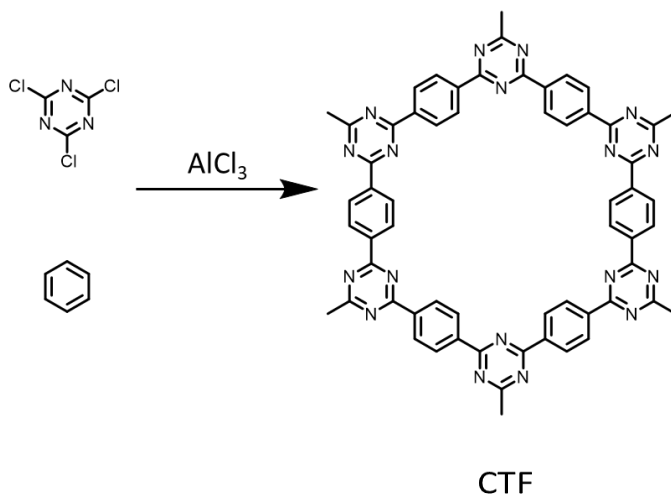


Figure 1.4 Structure of covalent triazine framework (ref.44)

1.4.2.2 Covalent organic frameworks (COFs)

Covalent organic frameworks (COFs) are an important emerging class of porous organic polymer having particular pore size and crystalline nature. Due to the polymerization of organic building blocks in a particular plane, they generate highly ordered pores and crystallinity. COFs are constructed through covalent bonds between organic building blocks, following reversible reactions such as Schiff base reactions, boronate ester formation, etc. The unique ordered structure and uniform pores make them suitable for various applications such as in catalytic reactions, selective separation etc⁴⁷⁻⁵¹.

1.4.2.3 Hypercrosslinked polymers (HCPs)

Hypercrosslinked polymers (HCPs) are one subclass of porous organic polymers, constructed with a three-dimensional network structure with a

high degree of crosslinking polymeric chain⁵³. The HCPs are synthesized using various methods, such as Friedel-Crafts Alkylation, polycondensation, and Friedel-Crafts acylation, with a crosslinking step to form the interconnected polymeric network. HCPs are promising candidate in various applications due to their high surface area and predominant porosity⁵²⁻⁵⁴.

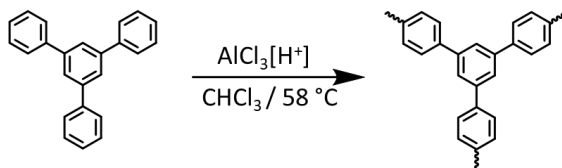


Figure 1.5 Structure of hypercrosslinked polymers (ref.44)

1.4.2.4 Conjugate microporous polymers (CMPs)

Conjugate microporous polymers (CMPs) are a fascinating class of porous organic polymers. They are synthesized by π -conjugated three-dimensional networks, using various coupling reactions, such as Suzuki coupling, Sonagasira coupling, or oxidative coupling. The conjugate nature of CMPs provides unique features like electronic conductivity and optical properties. This result could be utilized in various applications such as organic electronics, photovoltaic devices, light-emitting devices, and optoelectronics⁵⁵⁻⁵⁷.

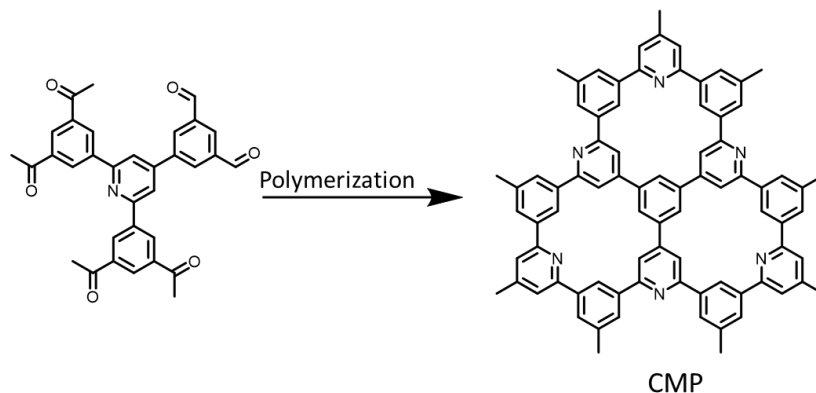


Figure 1.6 Structure of covalent microporous polymer (ref.44)

1.4.3 Classification of POPs on the basis of charge

Porous organic polymers (POPs) can be classified into two distinct categories based on their charge: neutral porous organic polymers and ionic porous organic polymers (iPOPs)⁵⁸.

1.4.3.1 Neutral porous organic polymers

Neutral porous organic polymers are a sub-class of porous organic polymers that are constructed through the repeated composition of neutral organic building blocks. As the name suggests, neutral porous organic polymers do not contain any charged functional groups. As shown in Figure 1.7, a neutral porous organic polymer has been synthesized by the combination of two neutral building blocks such as 2,4,6-tris(bromomethyl) phenyl)-1,3,5-triazine and p-xylylenediol (TTBr) and p-xylylenediol⁵⁹.

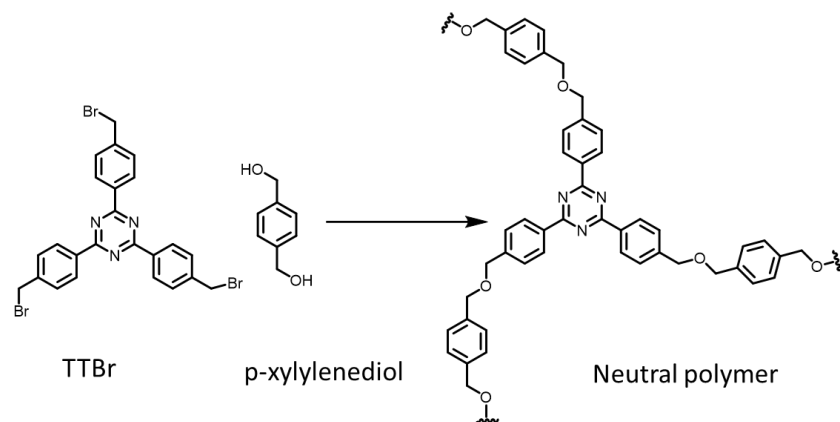


Figure 1.7 Synthetic diagram of a neutral porous organic polymer (ref.59)

1.4.3.2 Ionic porous organic polymers (iPOPs)

Ionic porous organic polymers are charged analogous to neutral porous organic polymers. The choice of suitable building blocks leads to the formation of a charged center in the polymeric skeleton. Ionic porous organic polymers could be synthesized by several methods: (1) using

building blocks with a charged center, (2) ionic polymerization, i.e., choosing building blocks that polymerize to create charged centers in the polymeric skeleton, (c) post-synthetic modification of the neutral polymers. Due to the presence of ionic characteristics, ionic polymers show unique properties such as ion exchange capability, strong electrostatic interactions with ions and polar molecules, electronic conductivity, etc. iPOPs also can be classified further into three subclasses (1) anionic porous organic polymers, i.e. it possesses anionic functionalities in its polymeric skeleton (2) cationic porous organic polymers, that having cationic centers in the skeleton and (3) zwitterionic porous organic polymers, that contains both the cationic and anionic centers in its skeleton⁶⁰⁻⁶².

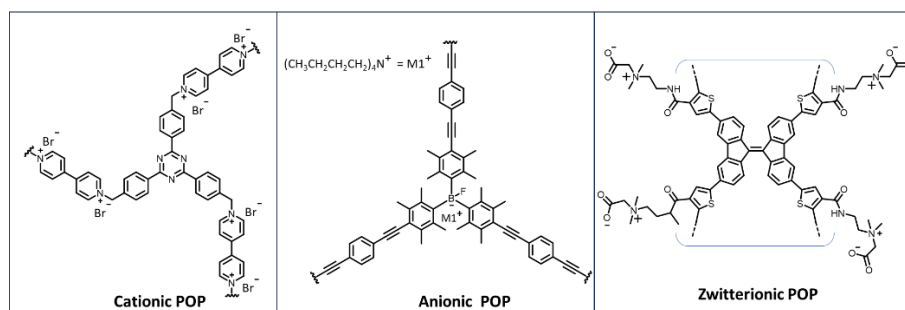
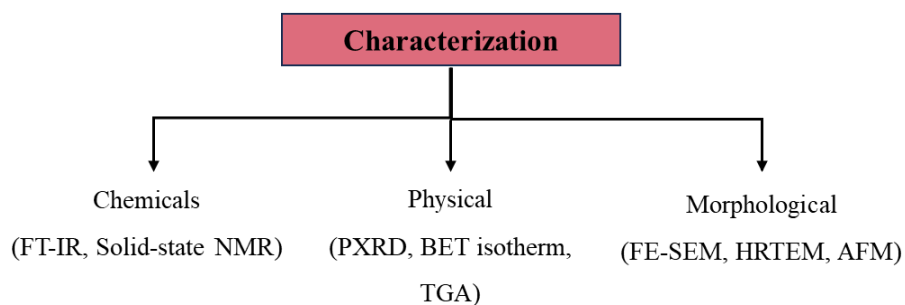


Figure 1.8 Structure of cationic (ref. 60), anionic (ref. 61) and zwitterionic (ref. 62) porous organic polymer.

1.5 Characterization of POPs

The porous organic polymers are characterized using several techniques:



1.5.1 Fourier-transform infrared spectroscopy (FT-IR)

The formation of polymers with the desired connectivity of different linkages is primarily supported by FT-IR stretching bands. It also helps to get information about the presence of different functional groups.

Some FT-IR stretching frequency of linkages are given in table 1.1

S.No.	Linkage	Stretching frequency ($\bar{\nu}$ cm ⁻¹)	Ref.
1	HL-COP, (-NH, -C=O, - C=N)	3429, 1672, 1549	63
2	iPOP-Bpy, (-CH ₂ ⁺ - aromatic -C=C-, triazene ring)	1408, 163, 61517 and 15	60
3	iPOP-ANT, (-C=N-, -CH ₂ , imidazolium)	1515, 1417, 1144 and 775	64
4	TpDAB, (-NH, -C=O, - C=C-)	3100-3300, 1612, 1598	65
5	AB-COF, -C=N-	1620-1630	66
6	POP-PU, (-C=O, -N-H and -C-N)	1632, 3299, 1220	67
7	COF-66, -C=N-	1620 and 1249	68

Table 1.1

1.5.2 Solid-state NMR

Solid-state nuclear magnetic resonance (NMR) spectroscopy is an extremely powerful technique for investigating the local environments and molecular structure of porous organic polymers (POPs). Due to their insolubility in deuterated NMR solvents, ¹³C cross-polarization magic angle spinning solid-state NMR spectroscopy is the preferred method for identifying the secondary building block in polymeric networks⁶⁹.

1.5.3 TGA (Thermogravimetric analysis)

Thermogravimetric analysis (TGA) is an essential technique used to analyze the thermal properties of porous organic polymers (POPs). The shape and size of the polymer significantly influence the thermal stability of POPs. In this analysis, the weight shift in a substance is monitored as a function of temperature in a controlled atmosphere⁷⁰.

1.5.4 BET

The Brunauer-Emmett-Teller (BET) isotherm is a valuable technique to analyze the specific pore structure, surface area, and pore distribution in the case of porous organic polymers (POPs). It is also used to analyze the adsorption behavior of porous organic polymers or porous materials. It describes the significant relation between the amount of gas adsorbed onto the material's surface at a specific temperature and the relative pressure of the gas. The BET equation is defined as-

$$\frac{1}{W \left(\left(\frac{P_0}{P} \right) - 1 \right)} = \frac{1}{W_m C} + \frac{C - 1}{W_m C} \left(\frac{P}{P_0} \right) P_0$$

Where W , P/P_0 , W_m , and C represent the weight of adsorbed gas, relative pressure, the weight of adsorbate as a monolayer, and BET constant⁷¹.

1.5.5 PXRD

Powder X-ray diffraction patterns provide information about the crystallinity nature or amorphous nature of porous organic polymers. The broad PXRD pattern indicates the amorphous nature of polymers while the Sharpe pattern indicates the crystalline nature of the polymers⁷².

1.5.6 FESEM

FE-SEM (Scanning Electron Microscopy) technique helps to get information about morphological aspects of porous organic polymers (POPs)⁷³.

1.6 Organization of the Thesis

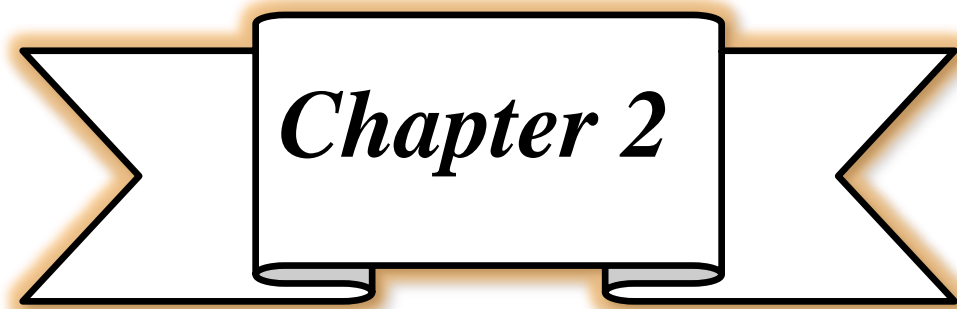
The motive of this project is the synthesis of ionic porous organic polymers (iPOPs) for the sense and removal of toxic pollutants from wastewater.

Chapter 2 This chapter discusses the literature survey and the previous lab work done in this field, which motivates this project.

Chapter 3 The experimental procedures of the synthesis of iPOPs and their application have been discussed in this chapter. The instruments used are also discussed in this chapter.

Chapter 4 The results obtained are discussed regarding the synthesis of iPOPs and their applications for detecting and removing metal-based oxoanions and toxic anionic dyes.

Chapter 5 The concluding and comprehensive overview of this project is provided along with the future plans.



Chapter 2

Literature Survey & Project

Motivation

2.1 Review of Past Work and Project Motivation

The porous organic polymers (POPs) are synthesized by combining organic building units by covalent linkages using simple organic reactions like Schiff base condensation, Friedel-craft alkylation reaction, Suzuki coupling reaction, aldol condensation, etc. In the synthesis of POPs, the organic building blocks are combined with the help of some general linkages like imine, hydrazone, azine, phenazine, -C-C- etc.

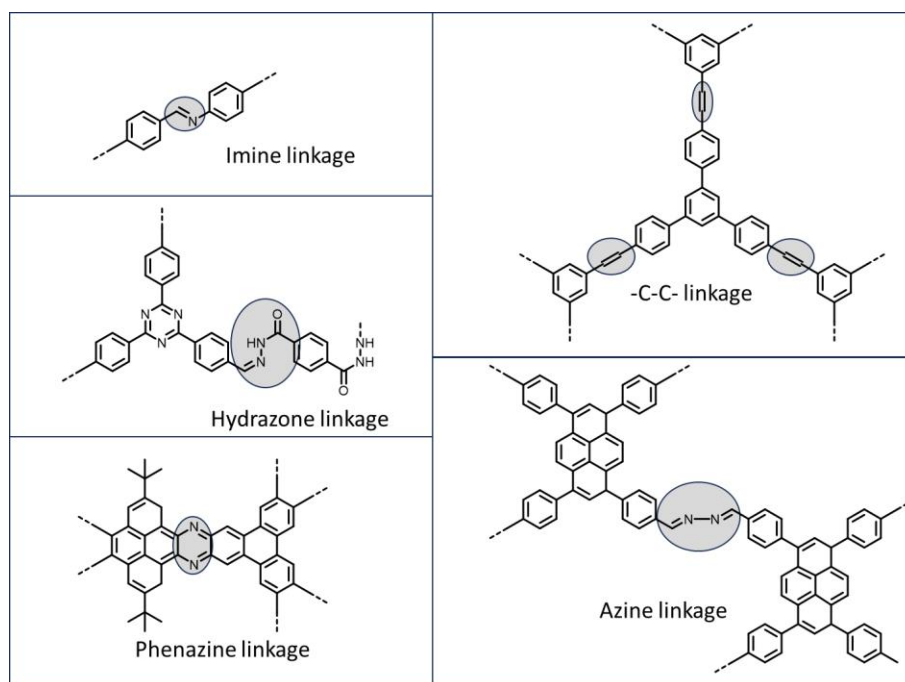


Figure 2.1 General linkages used in porous organic polymers

Considering the wastewater contaminants that mostly contain anionic pollutants such as $\text{Cr}_2\text{O}_7^{2-}$, TcO_4^- , AsO_4^- , CrO_4^{2-} , MO, amaranth, etc., choosing cationic porous organic polymers as a porous adsorbent will be helpful.

In the synthesis of cationic porous organic polymers, some building blocks have been used to generate cationic centers on the polymeric network. There are three ways to introduce a cationic center in the polymeric skeleton:

1. Choosing cationic building blocks as one of the building units.
2. Building units that will react among themselves during polymerization will be considered to generate cationic sites in the polymeric skeleton.
3. Post-synthetic modification of neutral polymers chemically to generate a cationic center in the polymer⁷⁴.

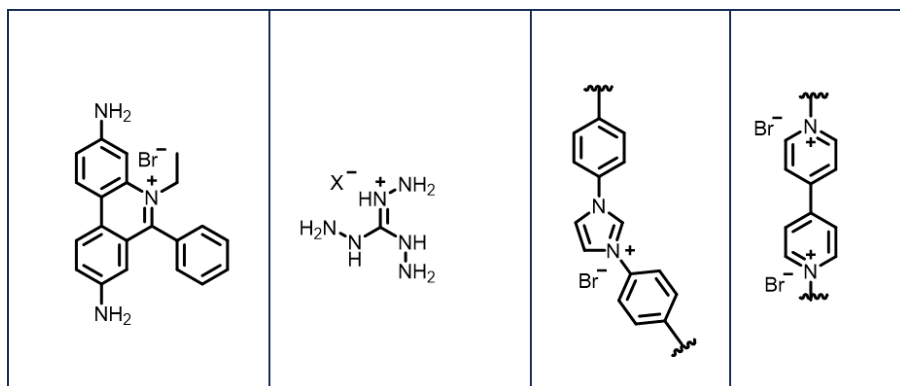


Figure 2.2 Known examples of building blocks/groups used in cationic porous organic polymers⁷⁵.

Among all the building blocks, several building blocks containing porous organic polymers are not suitable for water remediation due to their compromised stability in harsh wastewater conditions. For example, Viologen and their derivative-containing polymers due to their redox-switching nature at higher pH lose significant cationic sites at higher pH, thereby significantly losing their adsorption capability. Imidazolium or guanidinium containing porous organic polymer has shown to have very high acid and base tolerance in extreme pH and could be efficient candidates for industrial wastewater remediation. The presence of the imidazolium group in the ionic porous organic polymers (iPOPs) network plays a significant role in capturing anionic pollutants. Imidazolium and guanidinium iPOPs are known candidates in the field of wastewater remediation and have proven their significance in capturing a wide range of oxo-anions and anionic dyes from wastewater. Their N-rich pre-modified positively charged centers enhance the cationic environment on the polymeric

network and help selectively capture anionic pollutants through electrostatic interactions.

There are several reports where various imidazolium and guanidinium groups containing porous organic polymers have been used for the removal of ionic contamination from contaminated water. Sarkar et al. developed imidazolium and viologen-based ionic Porous Organic Polymers (iPOP-ANT and iPOP-BPY) and used them as adsorbent sponges in the efficient capture of several toxic inorganic and organic pollutants^{60,64}. Jiao et al. also developed imidazolium and triazene-based iPOPs (QUST-iPOP-1) and used them in the selective adsorption of several anionic dyes from a mixture of cationic and anionic dyes⁷⁶. Recently, Li et al. reported an imidazolium-based moiety containing a porous organic polymer, which showed excellent selectivity and outstanding adsorption performance in TcO_4^- . Liu et al. also reported the development of imidazolium-based iPOPs and their use in scavenging anionic radioactive impurities from water⁷⁷. In the latest report by Chandra et al., a guanidinium-based ionic porous organic polymer, which shows good adsorption capacity toward various inorganic and organic species such as CrO_4^{2-} , TcO_4^- , I_3^- , diclofenac, and picrate⁷⁸. Santa *et al.* prepared a guanidinium-based ionic porous organic polymer to remove Cr (IV) oxoanions from wastewater⁷⁹. According to the above-mentioned reports, the presence of the cationic centers containing groups (imidazolium and guanidinium) in the skeleton of the cationic polymeric network enhances the selectivity and scavenging capacity toward anionic pollutants. Therefore, integration of imidazolium and guanidinium sites in the same polymer might prove to be more advantageous as it will increase the number of cationic centers in the polymer.

In designing high-performance iPOPs-based porous adsorbent, the charge density might play a very significant role. But this factor always gets ignored while designing iPOP-based porous adsorbent.

Charge density around the binding sites of iPOPs could be easily manipulated by simply changing the secondary building blocks in the polymers. Keeping this hypothesis in mind, three imidazolium and guanidinium-based cationic porous organic polymers (iPOP-IMZ-1, iPOP-IMZ-2, and iPOP-IMZ-3) have designed and synthesized to optimize the effect on adsorption of anionic pollutants due to increasing distance between two adjacent cationic centers and increasing cationic center density in the polymeric network and detection of heavy metal-based contaminations.

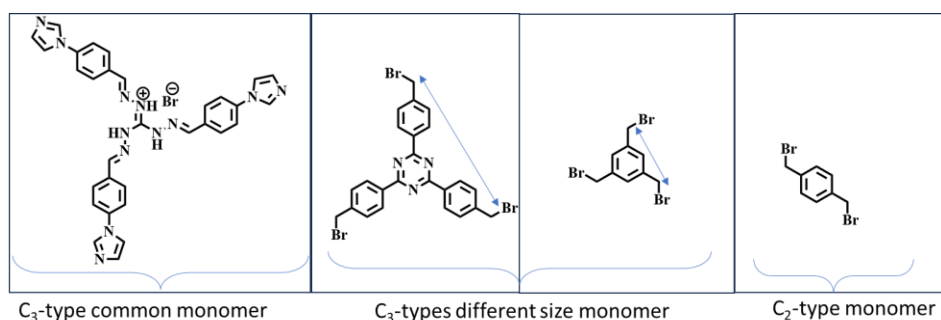
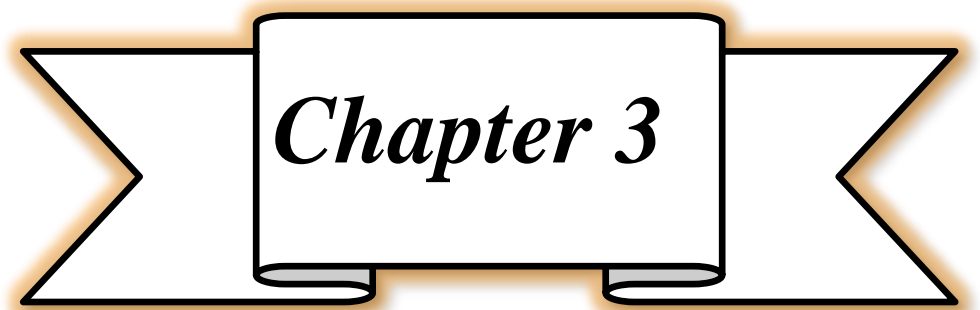


Figure 2.3 The structure of the different types of monomers used to make the polymers used in this work.

In the synthesis of iPOP-IMZ-1 and iPOP-IMZ-2, two C_3 -type monomers of different sizes were considered, whereas to check the role of symmetry a C_2 -type building block was used in designing iPOP-IMZ-3. A common imidazolium and guanidinium-based C_3 type monomer was considered as a charged building block in the whole study. The luminescent nature of polymers (iPOP-IMZ-2 and iPOP-IMZ-3) would be helpful in selectively detecting heavy metal-based contaminations.



Chapter 3

EXPERIMENTAL SECTION

3.1 Reagent & Chemicals

Guanidine nitrate, methyl orange (MO), amaranth, and rhodamine-B (RhB) were purchased from AVRA chemicals. α , α' dibromo *p*-xylene, and 4-fluorobenzaldehyde, 4-(bromomethyl)benzotrile were purchased from Sigma-Aldrich. Methylene Blue (MLB) was purchased from Spectrochem. Tryoctyleammonium chloride, 1,3,5 tris bromomethyl benzene were purchased from BLD Pharm. Triflic acid, DMSO, Dioxane, methanol, acetone, DCM, and chloroform were purchased from FINAR. $K_2Cr_2O_7$ and $KMnO_4$ were purchased from MERK.

3.2 Instrumentation and Methods

The AVANCE NEO500 Ascend Bruker BioSpin international AG equipment with TMS as the standard reference was utilized to record the 1H NMR and ^{13}C NMR spectra. Fourier Transfer Infrared (FTIR) spectra were recorded on a Bruker Tensor 27 FTIR spectrometer (range: 4000 to 500 cm^{-1}). For analysis of absorption spectra, a PerkinElmer UV-vis spectrometer in a quartz cuvette (1 cm \times 1 cm) was used. Supra55 Zeiss Field emission scanning electron microscopy (FE-SEM) was used to capture the morphological image. Autosorb iQ2 Brunauer-Emmett -Teller (BET) surface area analyzer was used for the porosity parameters Quantachrome. PXRD data was recorded on the Empyrean, Malvern Panalytical, with $Cu-K\alpha$ radiation. TGA data were recorded on the Mettler Toledo Thermal Analyser with a heating rate of 10 $^{\circ}C$. Fluoromax-4 was used to record the fluorescence spectra.

3.3 Synthesis of the monomers

3.3.1 Synthesis of triaminoguanidinium nitrate:

A round-bottom flask was charged with 0.305 g (2.5 mmol) of guanidine nitrate in 6 mL of dioxane. It was followed by the addition of 0.5 mL (10.2 mmol) $NH_2NH_2.H_2O$. The whole solution was refluxed at 100 $^{\circ}C$ for 2 h.

The obtained white precipitate was filtered, washed with dioxane and ethanol, and then dried at 60° C for 24 h to get the product. Yield: 62% (Scheme 4.1)⁸⁰.

3.3.2 Synthesis of 4-imidazolyl-benzaldehyde:

In a round bottom flask, 0.68 g (10 mmol) of imidazole, 1.38 g (10 mmol) of anhydrous potassium carbonate, 1.24 g (10 mmol) of 4-fluorobenzaldehyde, and two drops of trioctylmethylammonium chloride were taken in 20 mL DMF. The reaction mixture was stirred for 24 h at 85° C. The reaction mixture was stirred for 24 h at 85° C. The pale-yellow lamellar crystals were obtained immediately after the room temperature-cooled mixture was poured into ice water subsequent to the completion of the reaction. The product was filtered and dried. Yield: 66.3%; (Scheme 4.2)⁸¹.

3.3.3 Synthesis of GID.HNO₃

An oven-dried round bottom flask was charged with 0.3g (1.795 mmol) of triaminoguanidinium nitrate dissolved in 10 mL of water. A solution of 1.080g (6.28 mmol) of 4-(1H-Imidazol-1-yl) benzaldehyde in 15 mL ethanol was added dropwise in an aqueous solution of triaminoguanidinium nitrate and allowed to reflux for 24h. The yellow precipitate was collected by filtration and washed thoroughly with ethanol and acetone. Finally, the residue was dried under a vacuum to get the GID.HNO₃ as a yellow powder. Yield: 82% (0.92g); (Scheme 4.3)⁸².

3.3.4 Synthesis of 2,4,6-tris(-(bromomethyl) phenyl)-1,3,5-triazine (TTBr)

An oven-dried 50 mL two-neck round bottom flask was charged with 2.0 g (10.2 mmol) of 4-bromomethylbenzonitrile and placed in an ice bath. To it, CF₃SO₃H (3.0 mL, 33.90 mmol) was added dropwise for 2 h under the N₂ atmosphere and allowed to stir for another 30 minutes. The reaction mixture was allowed to stir at room temperature for another 24 h after removing the

ice bath. After completion of the reaction, the reaction mixture was added to ice-cold water and neutralized with a dropwise addition of aq. NH_3 . The obtained precipitate was filtered and dried under a vacuum to obtain the product as a white solid as the desired product. Yield: 92%; (Scheme 4.4)⁸³.

3.4 Synthesis of ionic porous organic polymers

To an oven-dried round bottom flask, 0.15 g (0.238 mmol) of GID.HNO_3 and 0.138 g (0.238mmol) of TTBr in 25 mL of DMF were taken, and the mixture was heated at 120° C under N_2 gas for 24 h. The obtained yellow precipitate was filtered and washed thoroughly with a large amount of DMF, H_2O , and MeOH, respectively. The solid was then dipped in a 1:1 mixture of methanol and chloroform overnight and then dried at 70° C for 24 h to obtain the final product (Scheme 4.5).

iPOP-IMZ-2 and iPOP-IMZ-3 were synthesized following the same procedure. In the synthesis of iPOP-IMZ-2, 0.3 g (0.48mmol) of GID.HNO_3 was reacted with 0.17 g (0.48mmol) of 1,3,5-tris(bromomethyl)benzene in 25 mL of DMF (Scheme 4.6), whereas in the case of iPOP-IMZ-3, 0.3 g (0.48 mmol) of GID.HNO_3 and 0.189g (0.72mmol) of α,α' -dibromo-p-xylene were taken (Scheme 4.7).

3.5 Adsorption Study

3.5.1 Procedures of time-dependent study of anionic contamination adsorption from aqueous solution using synthesized iPOPs

To analyze the time-dependent adsorption study of metal oxo-anions and toxic anionic dyes, $\text{Cr}_2\text{O}_7^{2-}$ and MnO_4^- were considered as model oxo-anions, and methyl orange (MO) and amaranth were taken as model anionic dyes. In this experiment, 0.015 g of synthesized iPOPs were dispersed in 30 mL of 0.5 mM aqueous solution of oxo-anions and 30 mL 50 ppm aqueous solution of toxic anionic dyes. The resultant mixtures were stirred at room temperature and the supernatant was monitored under UV-vis spectroscopy

at different time intervals. The removal percentage was determined using the following equation

$$D_t = \frac{C_0 - C_t}{C_0} \times 100\% = \frac{A_0 - A_t}{A_0} \times 100\%$$

where D_t represents the exchange capacity, C_0 , and A_0 denote the initial concentration and absorbance of the anionic contaminant solution, and C_t and A_t signify the concentration and absorbance of the anionic contaminant solution at specific times.

The adsorption kinetics for removing anionic contamination were fitted in the pseudo-second-order model using the following equation

$$Q_t = \frac{K_2 Q_e^2 t}{1 + K_2 Q_e t}$$

where the time intervals are measured in minutes and represented by 't' while Q_t and Q_e represent the adsorbate (mgg^{-1}) amounts on the adsorbent at different time intervals and equilibrium, respectively.

3.5.2 Calculation of adsorption capacity of iPOPs towards oxo-anions and anionic dyes.

To calculate the uptake capacity of iPOPs, 5 mg of the desolvated iPOPs were depressed in a 10 mL solution of different concentrations of oxo-anions and dyes and stirred for 12 h. The adsorption capacity of iPOPs was calculated using the following equation:

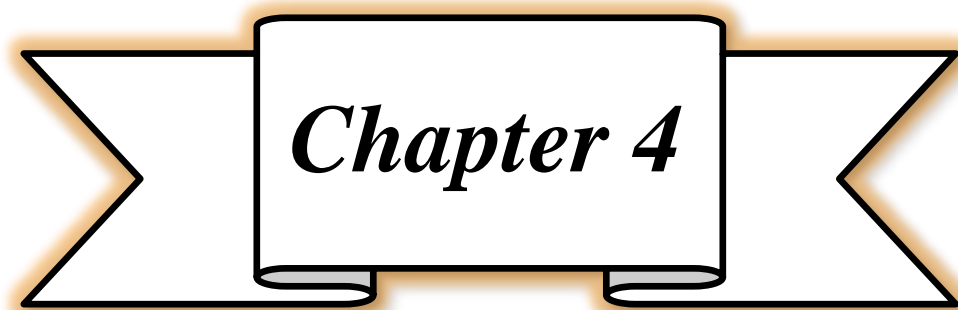
$$Q_e = \frac{Q_m C_e}{K_d + C_e}$$

where, C_e (mM), Q_e (mgg^{-1}), and Q_m (mgg^{-1}) represent the concentration of contamination, amount of contamination adsorbed at equilibrium and maximum amount of contaminant per unit mass of adsorbent respectively. K_d (mgmL^{-1}) represents a constant related to the affinity of binding sites.

3.6 Sensing study

3.6.1 Fluorescence sensing $\text{Cr}_2\text{O}_7^{2-}$ and MnO_4^- by using iPOPs

To analyze the sensing activities of iPOPs, 3 mg of iPOPs (iPOP-IMZ-2 and iPOP-IMZ-3) was added to 3 mL of the aqueous solution of different concentrations (10 ppm - 100 ppm) of $\text{Cr}_2\text{O}_7^{2-}$ and MnO_4^- respectively. The mixtures were immediately investigated by measuring fluorescence. In this study, polymer iPOP-IMZ-1 wasn't used due to its nonfluorescent nature.



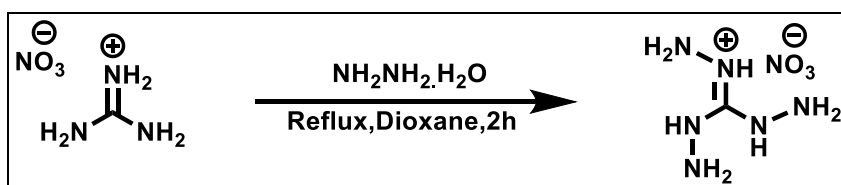
RESULTS & DISCUSSION

4.1 Structure and Synthesis

Three ionic Porous Organic Polymers, iPOP-IMZ-1, iPOP-IMZ-2, and iPOP-IMZ-3 have been synthesized by reacting GID.HNO_3 with 2,4,6 tris((bromomethyl)phenyl)1,3,5 triazine, 1,3,5 tris(bromomethyl)benzene and p-dibromoxylene in DMF (Scheme 6.2.5, 6.2.6 and 6.2.7). The successful synthesis of the products was confirmed by FTIR spectroscopy.

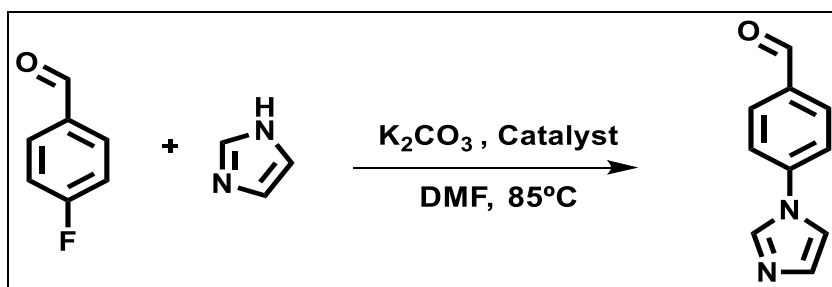
4.2 Reaction Schemes

4.2.1 Synthesis of triaminoguanidinium nitrate



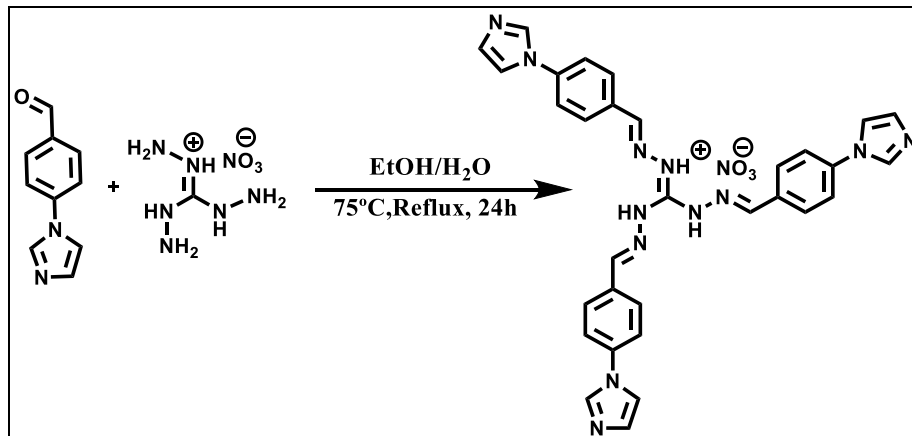
Scheme 4.1: Reaction Scheme for Synthesis of triaminoguanidinium nitrate

4.2.2 Synthesis of 4-imidazolyl-benzaldehyde



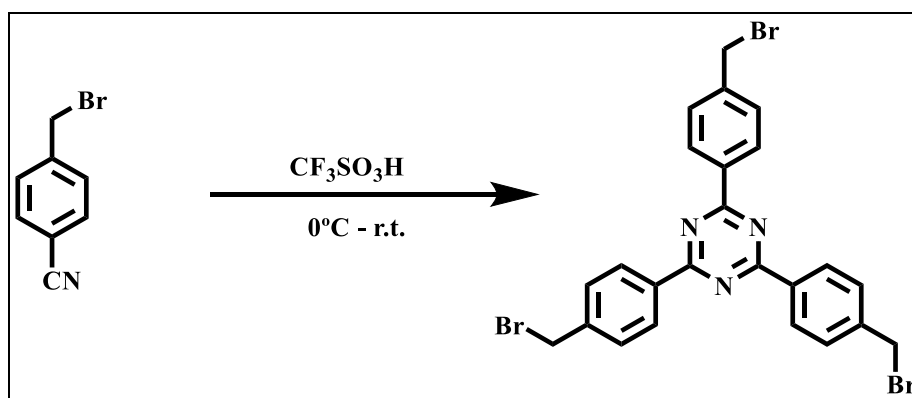
Scheme 4.2: Reaction Scheme for Synthesis of 4-imidazolyl-benzaldehyde

4.2.3 Synthesis of *GID.HNO₃*



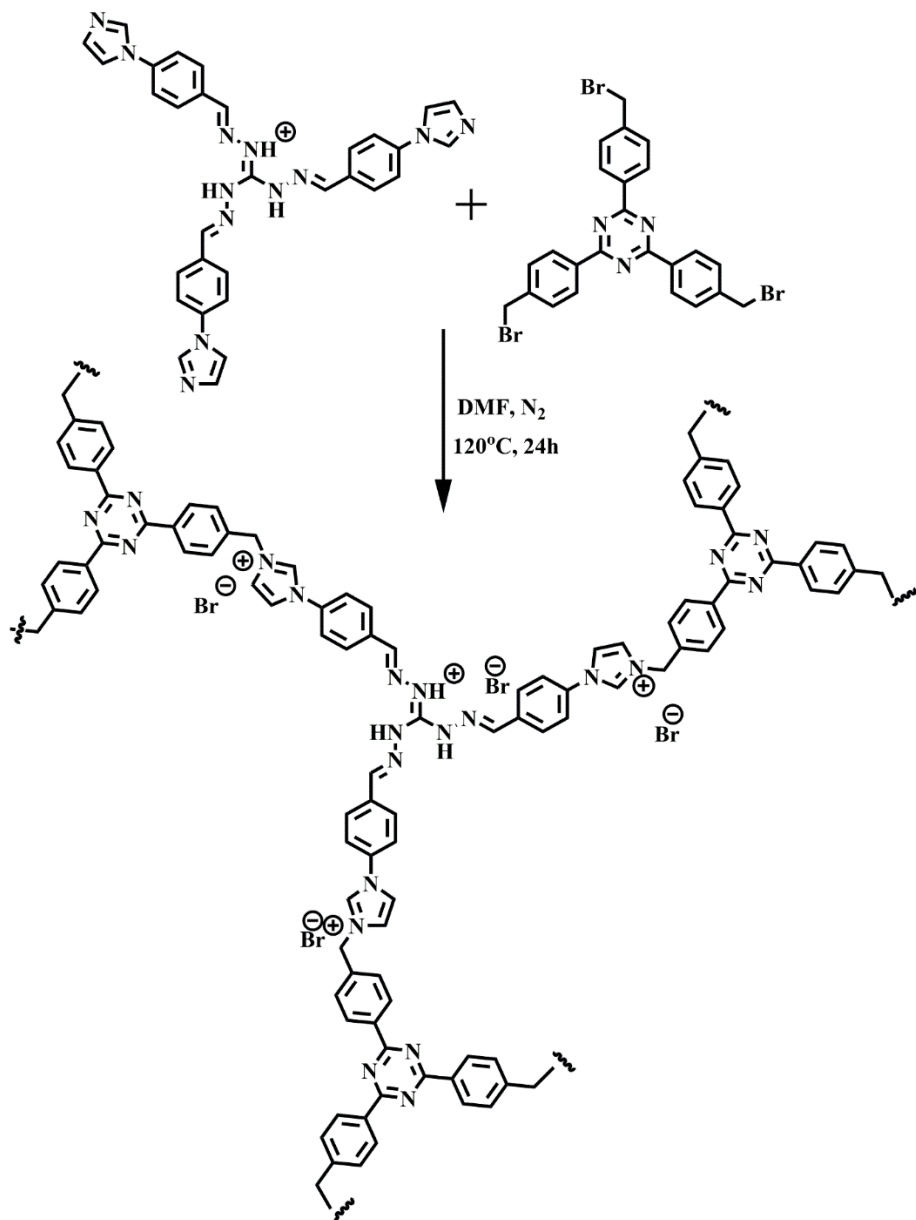
Scheme 4.3: Reaction Scheme for Synthesis of GID.HNO₃

4.2.4 Synthesis of 2,4,6-tris (-(*bromomethyl*) phenyl)-1,3,5-triazine (*TTBr*):



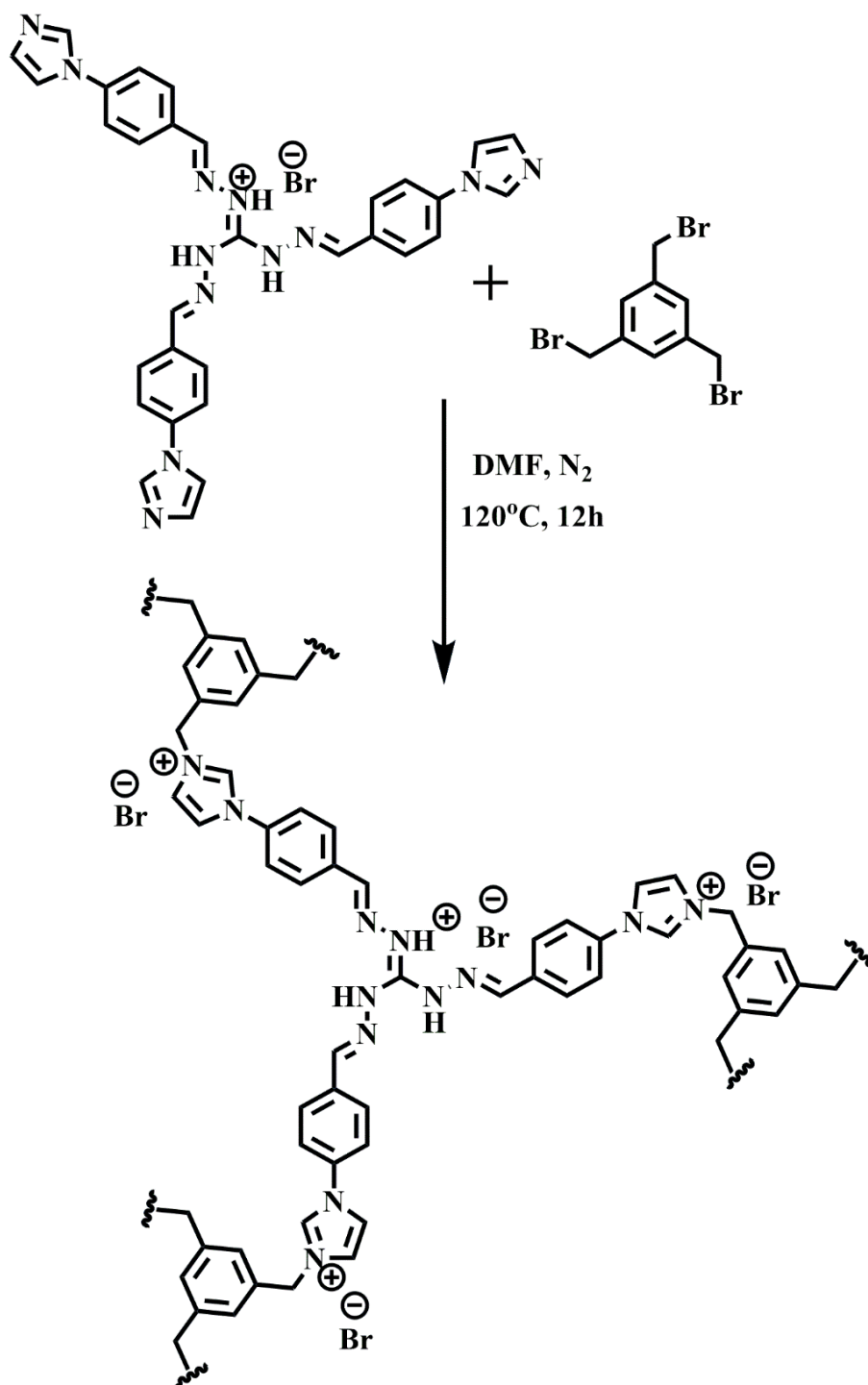
Scheme 4.4: Reaction Scheme for Synthesis of 2,4,6-tris(bromomethyl)phenyl-1,3,5-triazine

4.2.5 Synthesis of iPOP-IMZ-1



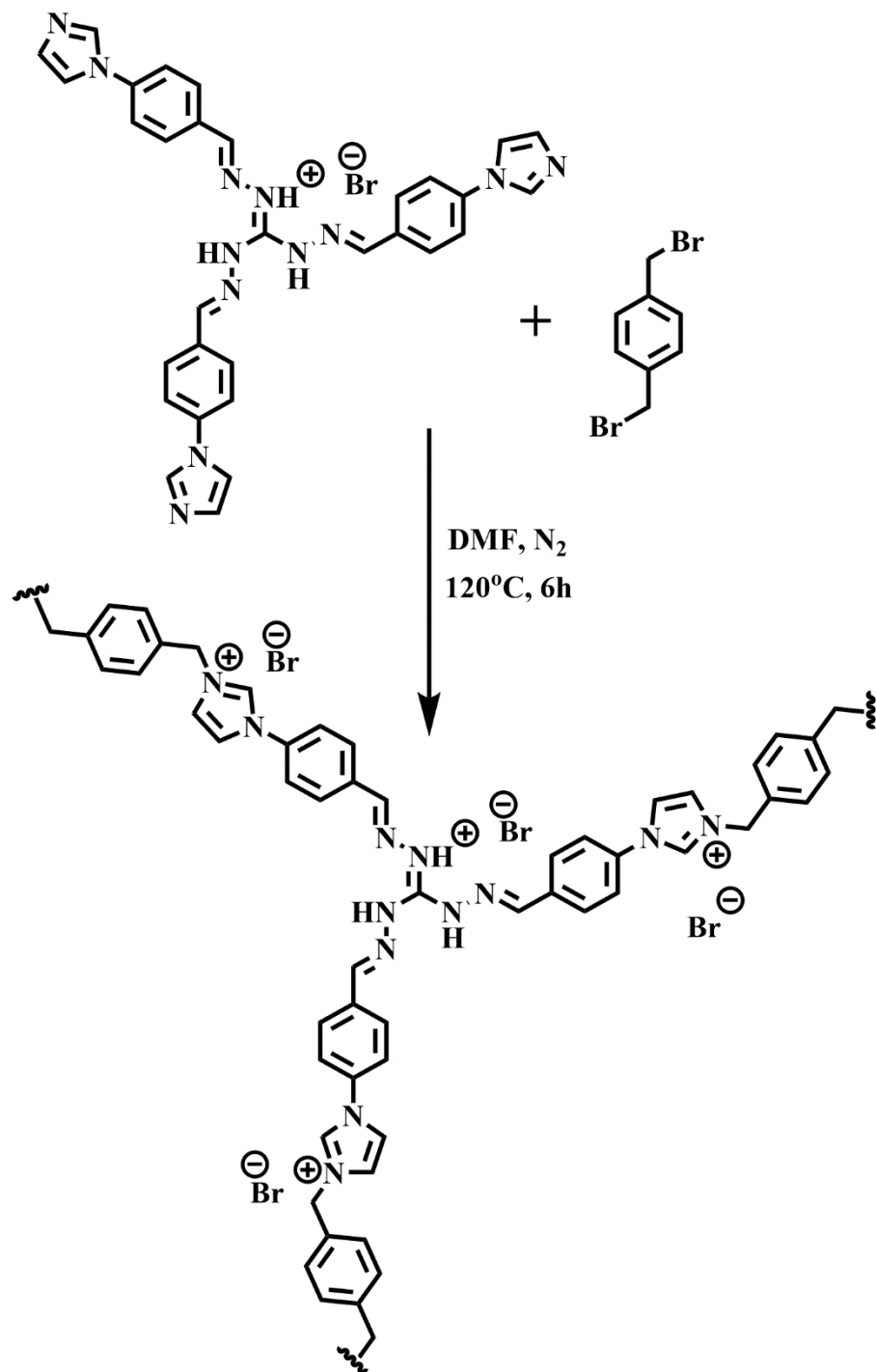
Scheme 4.5: Reaction Scheme for Synthesis of iPOP-IMZ-1

4.2.6 Synthesis of iPOP-IMZ-2



Scheme 4.6: Reaction Scheme for Synthesis of iPOP-IMZ-2

4.2.7 Synthesis of *iPOP-IMZ-3*



Scheme 4.7: Reaction Scheme for Synthesis of iPOP-IMZ-3.

4.3 Characterisation

4.3.1 Characterisation of starting material of pops

4.3.1.1 NMR Spectra of triaminoguanidinium nitrate

NMR data for Triaminoguanidine nitrate matched with the reported data. ^1H NMR (500 MHz, DMSO- d_6): δ 8.58(s, 2H), 4.49(s, 4H), 3.35(s, 2H) ppm. ^{13}C NMR: δ 159.49 ppm (Figures 1 and 2).

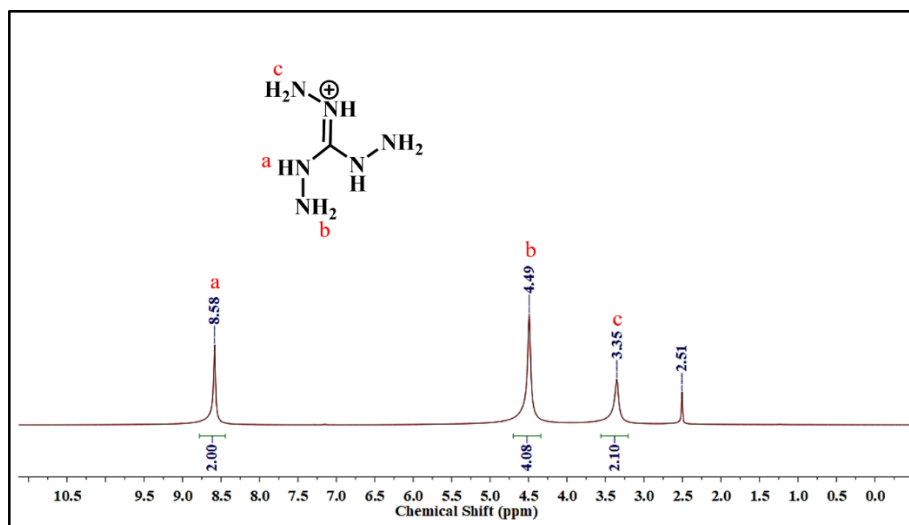


Figure 4.1: ^1H NMR of triaminoguanidinium nitrate

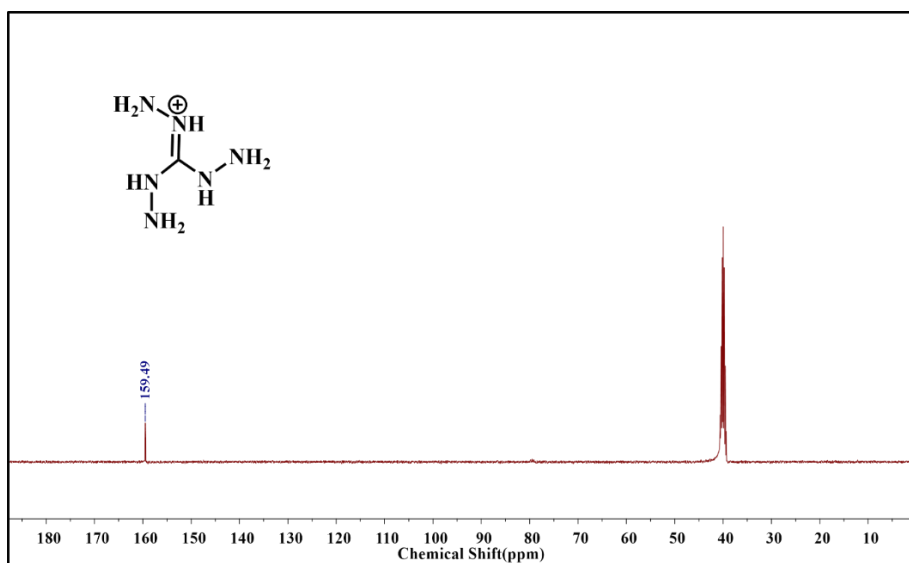


Figure 4.2: ^{13}C NMR of triaminoguanidinium nitrate

4.3.1.2 NMR Spectra of 4-imidazolyl-benzaldehyde

NMR data for 4-imidazolyl-benzaldehyde also matched with the reported data. ^1H NMR (500 MHz, DMSO-d_6): δ 10.04(s, 1H), 8.47(s, 1H), 8.06(d, 2H), 7.94(d, 2H), 7.14(s, 1H). ^{13}C NMR: δ 192.47, 141.67, 136.31, 134.69, 131.82, 131.01, 120.64, 118.27 ppm (Figures 3 and 4).

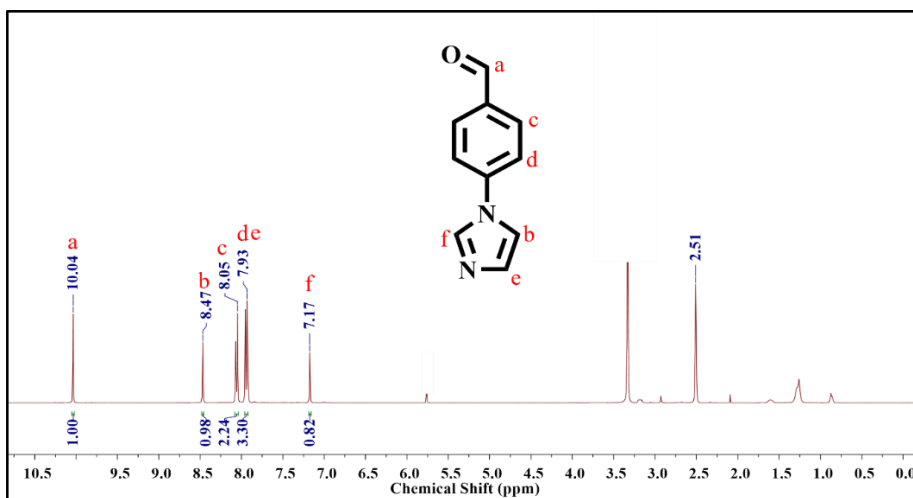


Figure 4.3: ^1H NMR 4-imidazolyl-benzaldehyde

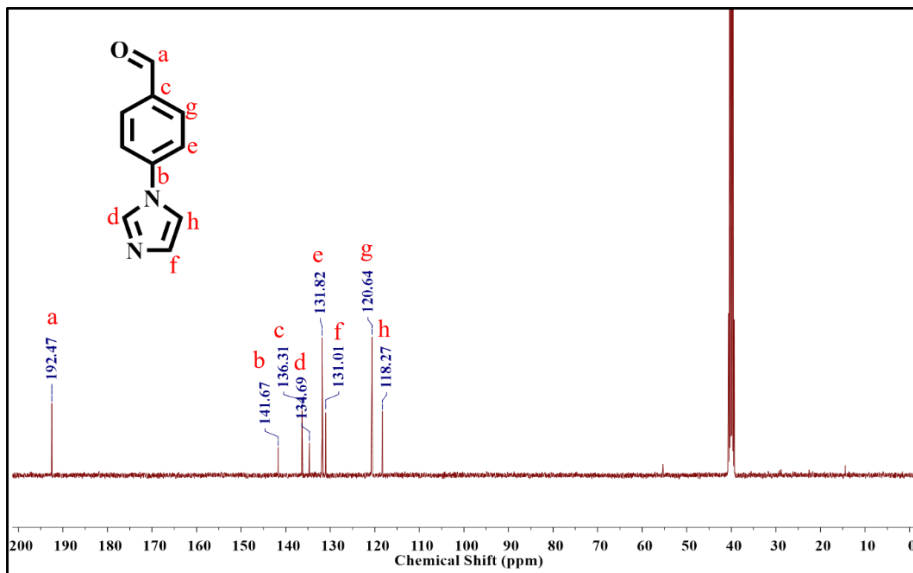


Figure 4.4: ^{13}C NMR of 4-imidazolyl-benzaldehyde

4.3.1.3 NMR Spectra of GID.HNO_3

NMR data for GID.HNO_3 also matched with the reported data. ^1H NMR (400 MHz, DMSO-d_6) δ : 8.75 (s, 3H), 8.57 (s, 3H), 8.15 (d, 6H), 7.96 (s, 1H) 7.88 (d, 6H), 7.26 (s, 3H) ppm (Figure 5).

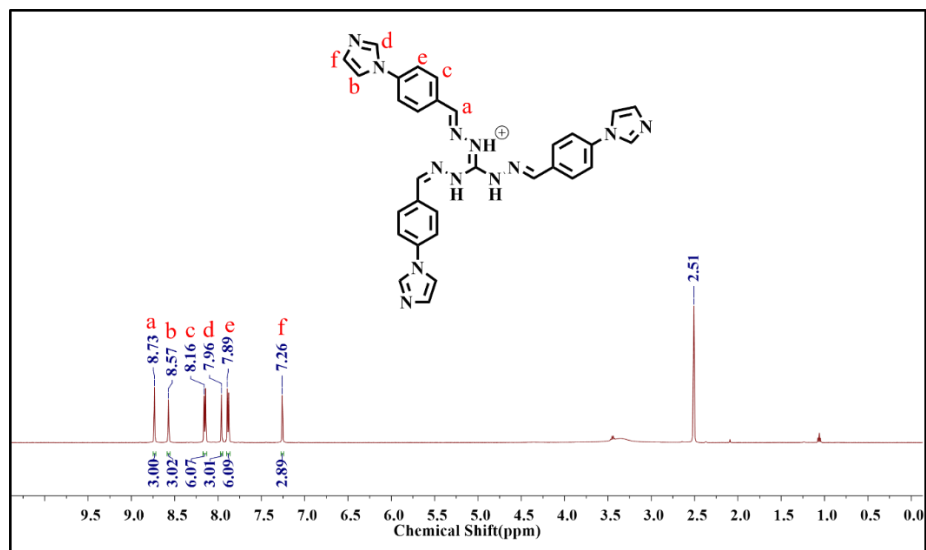


Figure 4.5: ^1H NMR of GID.HNO_3

4.3.1.4 NMR Spectra of 2,4,6-tris (-(*bromomethyl*) phenyl)-1,3,5-triazine (TTBr):

NMR data for 2,4,6-tris (-(*bromomethyl*) phenyl)-1,3,5-triazine (TTBr) also matched with the reported data. ^1H NMR (400MHz, CDCl_3): δ (ppm) 8.71(d, 6H), 7.59(d, 6H), 4.59(s,6H). ^{13}C NMR: δ 166.42, 137.55, 131.35, 124.70, 124.63, 27.96 ppm (Figure 6 and 7).

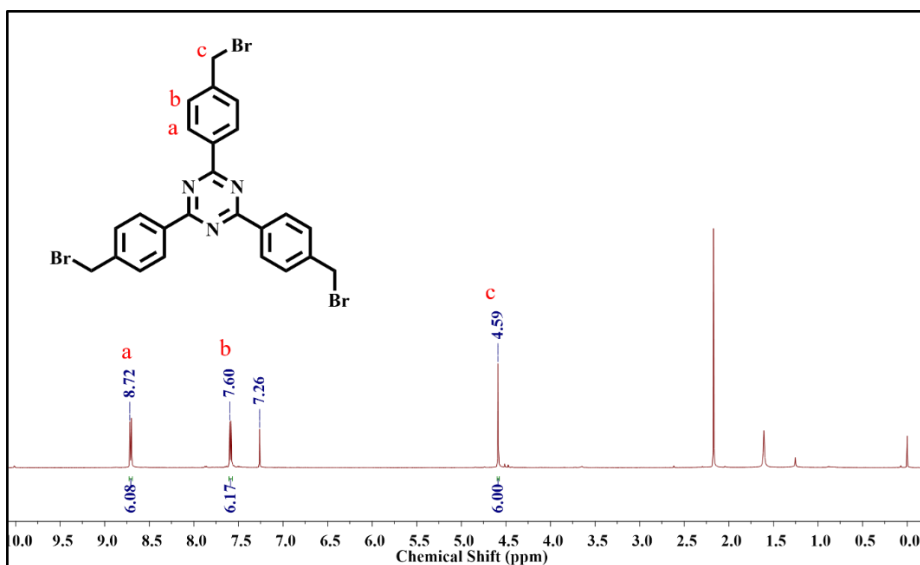


Figure 4.6: ^1H NMR of 2,4,6-tris(-bromomethyl)phenyl-1,3,5-triazine

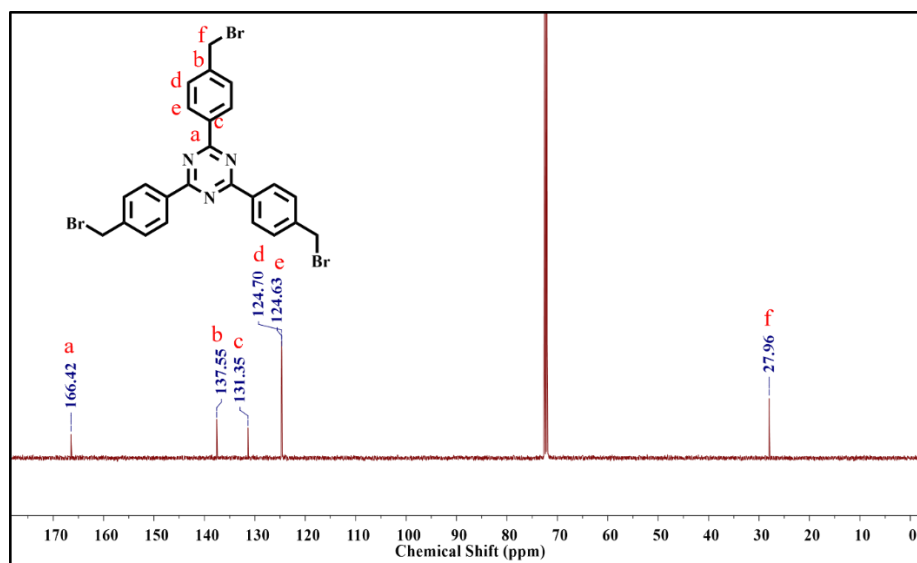


Figure 4.7: ^{13}C NMR of 2,4,6-tris(-bromomethyl)phenyl-1,3,5-triazine

4.3.2 Characterization of iPOPs

4.3.2.1 FTIR Spectra

In the FTIR spectra, the disappearance of C-Br stretching bands at 595 cm^{-1} , 574 cm^{-1} , and 608 cm^{-1} in iPOP-IMZ-1, iPOP-IMZ-2, and iPOP-IMZ-3,

respectively, represent the successful synthesis of the polymers. The bands at 752 cm^{-1} and 1187 cm^{-1} in iPOP-IMZ-1 and 742 cm^{-1} and 1114 cm^{-1} in iPOP-IMZ-2 and at 1192 cm^{-1} and 737 cm^{-1} in iPOP-IMZ-3 represent the presence of the imidazolium functionality in the polymers. The shift of $-\text{CH}_2-$ stretching frequencies from 1412 cm^{-1} to 1408 cm^{-1} in iPOP-IMZ-1, from 1436 cm^{-1} to 1413 cm^{-1} in iPOP-IMZ-2 and from 1419 cm^{-1} to 1410 cm^{-1} in iPOP-IMZ-3, confirms the formation of a cationic center in the polymer. In iPOP-IMZ-1, the bands 1364 cm^{-1} and 1515 cm^{-1} indicate the presence of triazine functionality in the polymer (Figure 8a-8c).

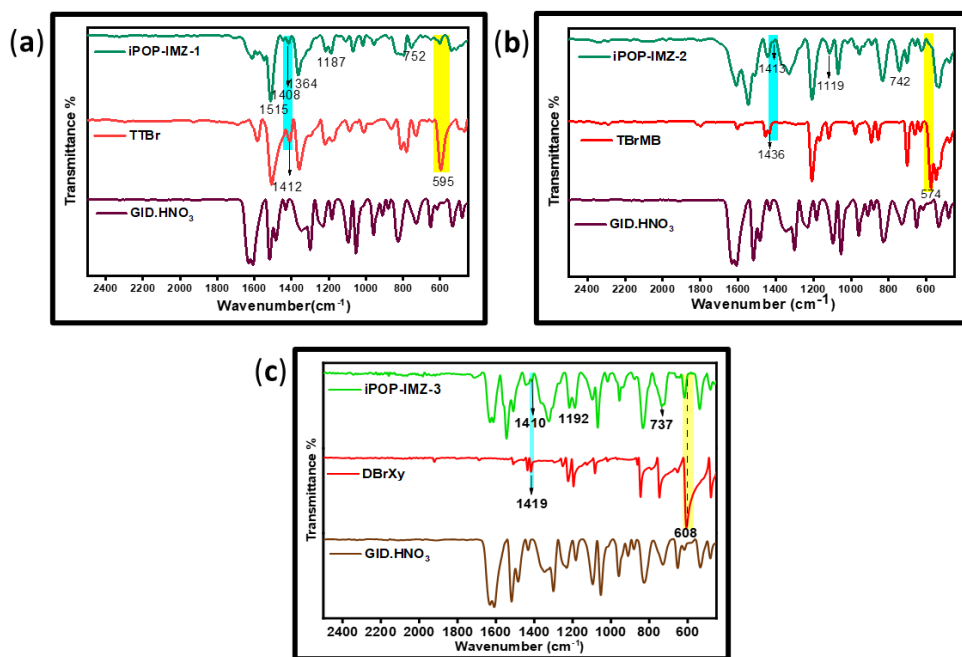


Figure 4.8 FTIR Spectra of (a) iPOP-IMZ-1 (b) iPOP-IMZ-2 and (c) iPOP-IMZ-3

4.3.2.2 Solid ^{13}C NMR Spectra

^{13}C CP/MAS NMR (Figures 9a-9c) spectra show distinct peaks due to present carbon in synthesized iPOPs, i.e., iPOP-IMZ-1, iPOP-IMZ-2, and iPOP-IMZ-3, respectively.

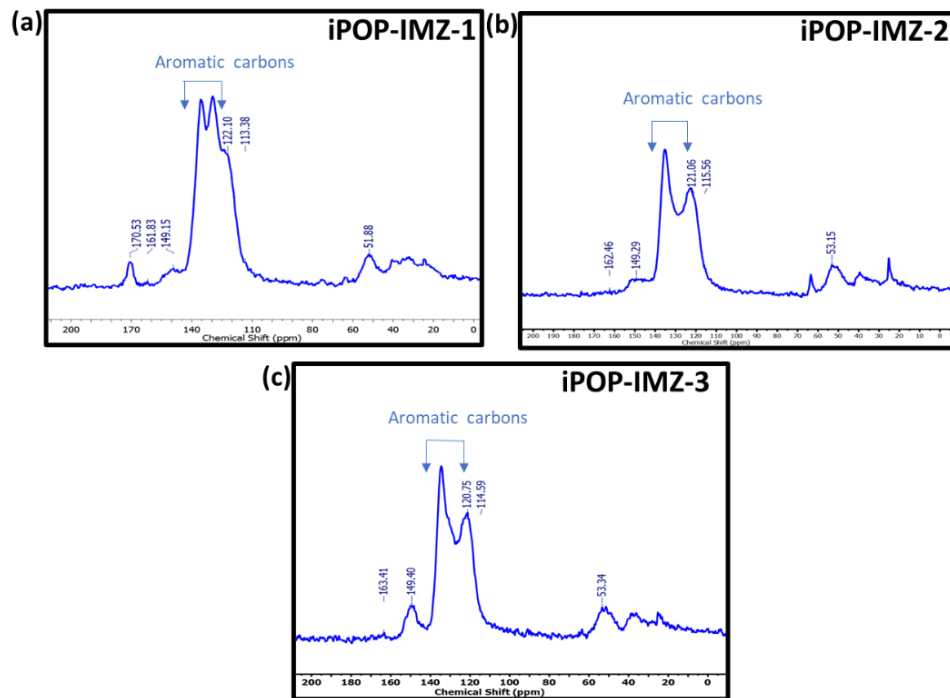


Figure 4.9 ^{13}C CP/MAS NMR for (a) iPOP-IMZ-1, (b) iPOP-IMZ-2, (c) iPOP-IMZ-3

4.3.2.3 TGA data

The thermal stability of the synthesized materials was investigated using thermogravimetric analysis (TGA). The TGA curves show that the materials are thermally stable up to 250°C (Figure 10).

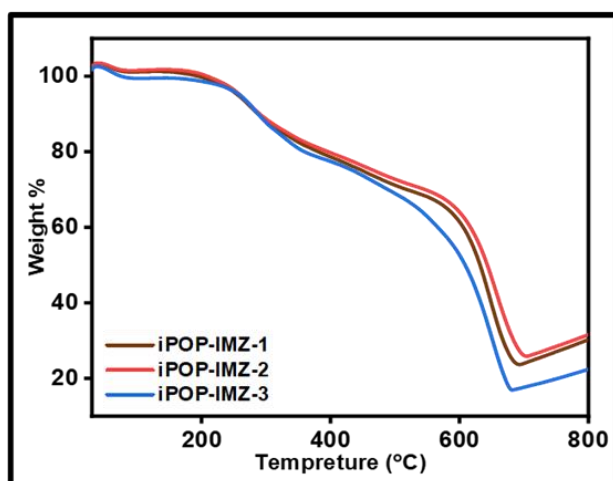


Figure 4.10 TGA curve of iPOP-IMZ-1, iPOP-IMZ-2 and iPOP-IMZ-3.

4.3.2.4 BET analysis

The porous characteristics of the as-synthesized materials were analyzed by Brunauer-Emmett-Teller (BET) isotherm through N₂ adsorption-desorption at 77K and 1 bar Pressure (Figure 11a). The BET surface areas were calculated to be 90.964, 240.604, and 50.205 m²/g for iPOP-IMZ-1, iPOP-IMZ-2, and iPOP-IMZ-3, respectively. The materials were found to be mesoporous, which was suggested through the pore size distribution curve (Figure 11b) as calculated from the BJH model.

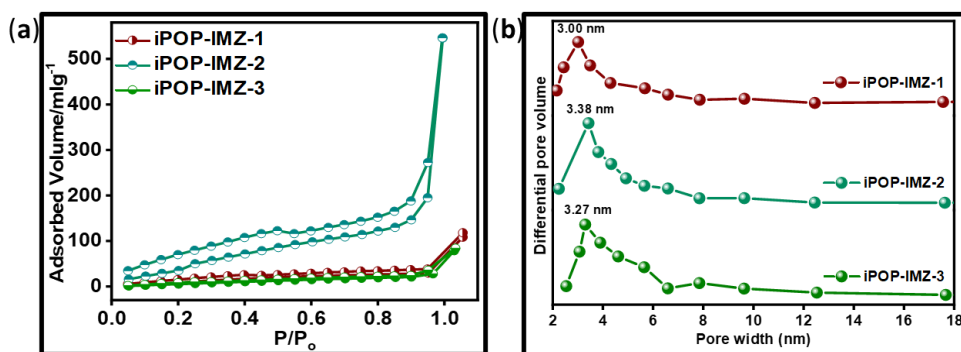


Figure 4.11 (a) N₂ adsorption isotherm and (b) Pore size distribution curve of iPOP-IMZ-1, iPOP-IMZ-2, and iPOP-IMZ-3 respectively.

4.3.2.4 PXRD data

The broad PXRD patterns (Figure 12a-12c) revealed that these ionic polymeric materials have an amorphous nature, which is quite common for these types of materials.

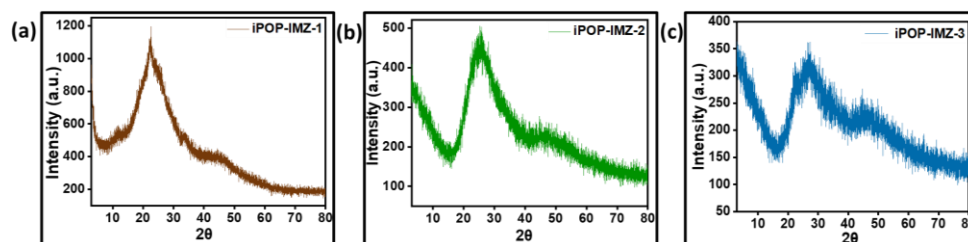


Figure 4.12 The PXRD pattern of (a) iPOP-IMZ-1, (b) iPOP-IMZ-2 and (c) iPOP-IMZ-3

4.3.2.4 FESEM Analysis

The synthesized iPOPs were imaged using FESEM, revealing their morphology: tubular for iPOP-IMZ-1, spherical for both iPOP-IMZ-2 and iPOP-IMZ-3(Figure 13a-13c).

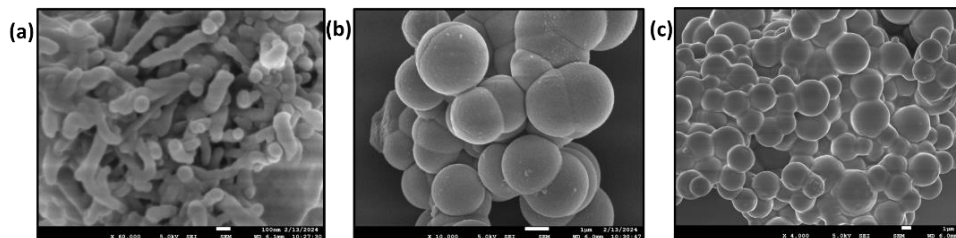


Figure 4.13 FE-SEM image of (a) iPOP-IMZ-1,(b) iPOP-IMZ-2, (c) iPOP-IMZ-3

4.3.2.4 EDX analysis

The EDX analysis of iPOPs reveals the presence of C, N and Br elements in every synthesized iPOPs (Figure14-16), and the mapping reveals information about the uniform distribution of presenting elements over the whole skeleton of iPOP-IMZ-1, iPOP-IMZ-2, and iPOP-IMZ-3(Figure17-19).

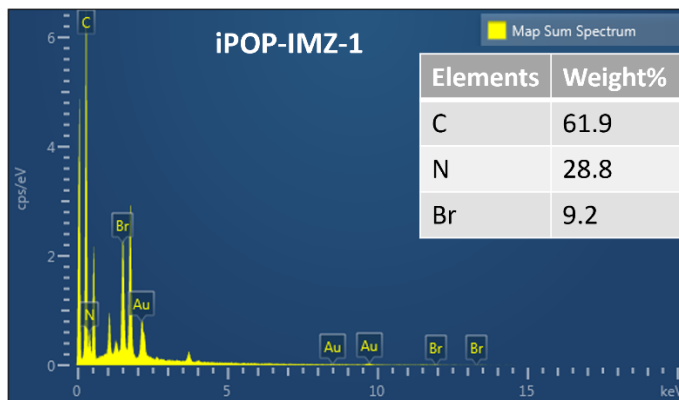


Figure 4.14 The EDX analysis of iPOP-IMZ-1

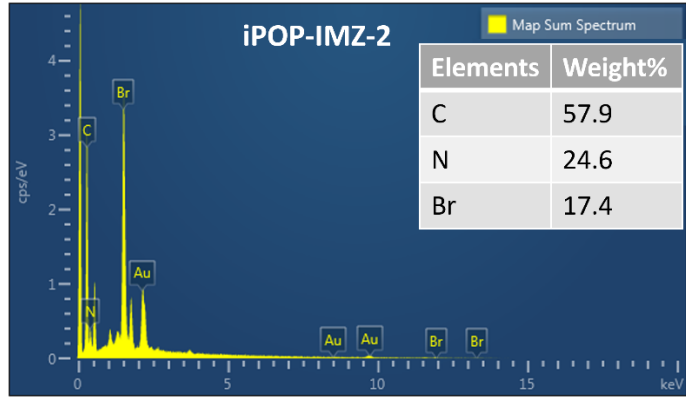


Figure 4.15 The EDX analysis of iPOP-IMZ-2

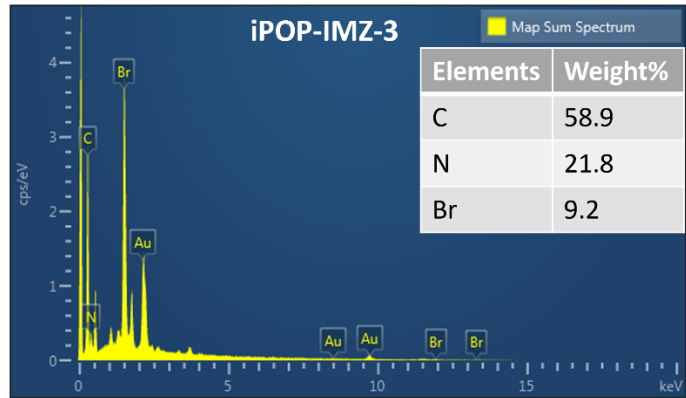


Figure 4.16 The EDX analysis of iPOP-IMZ-3

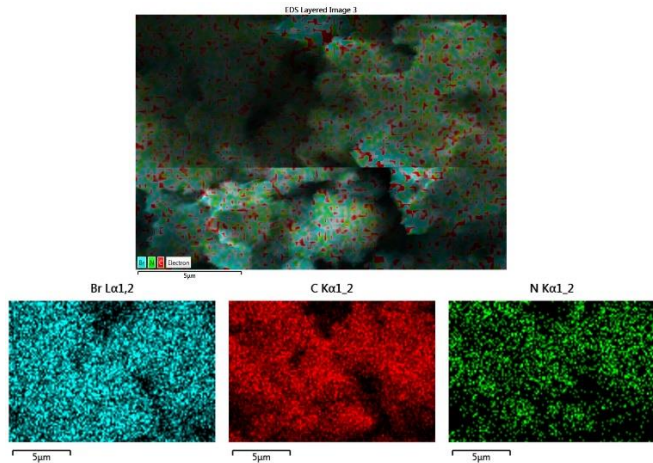


Figure 4.17 Mapping analysis of iPOP-IMZ-1

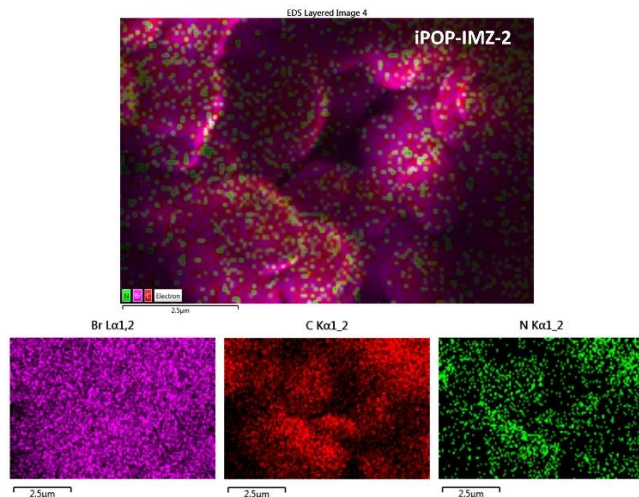


Figure 4.18 Mapping analysis of iPOP-IMZ-2

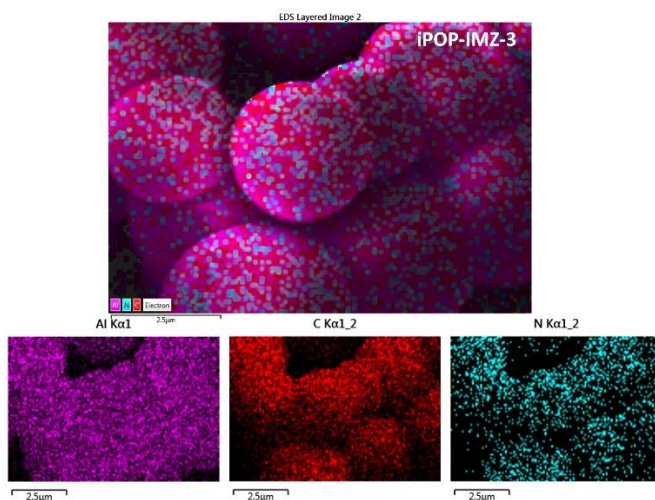


Figure 4.19 Mapping analysis of iPOP-IMZ-3

4.4 Analysis of adsorption of metal-based oxo-anions by iPOPs

Under the governance of UV-vis spectroscopy, the constant decrement of the characteristic peak at 258 and 352 nm for aqueous solution of $\text{Cr}_2\text{O}_7^{2-}$ in the presence of iPOP-IMZ-1(Figure 20a), iPOP-IMZ-2(Figure 20b) and iPOP-IMZ-3(Figure 20c) in 1 min time intervals indicate the rapid adsorption of $\text{Cr}_2\text{O}_7^{2-}$ by the polymers. As shown in Figures 20d and 20e, the steady decrease in the concentration of the aqueous solution of $\text{Cr}_2\text{O}_7^{2-}$

with time in the presence of iPOPs and adsorption reaches 92.5% for iPOP-IMZ-1, 98.5% for iPOP-IMZ-2 and 96.7% for iPOP-IMZ-3 within 5 min, 5 min, and 7 min respectively. Based on the analysis, the adsorption process was obtained to follow the pseudo-second-order kinetics with R^2 value 0.99 for iPOP-IMZ-1, 0.99 for iPOP-IMZ-2, and 0.98 for iPOP-IMZ-3 (Figure 20f).

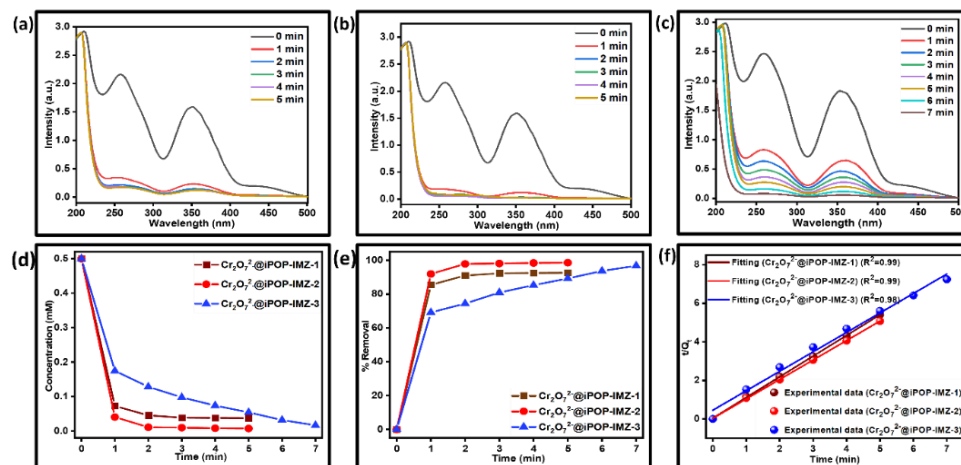


Figure 4.20 The UV-vis spectra, at different times for aqueous solution of $Cr_2O_7^{2-}$ in the presence of (a) iPOP-IMZ-1, (b) iPOP-IMZ-2, (c) iPOP-IMZ-3. (d) Decrease in the concentration and (e) removal (%), with time in the presence of iPOPs (f) The pseudo-second-order kinetics of the aqueous solution of $Cr_2O_7^{2-}$.

It's very difficult to operate TcO_4^- ions in the lab due to their radioactive nature; - that's why its nonradioactive surrogate MnO_4^- was chosen to check the adsorption ability of our materials towards radioactive TcO_4^- ions. In this analysis also, it has been observed that there is a constant decrement of the characteristic peak at 525nm (λ_{max}) for the aqueous solution of MnO_4^- in presence of polymers iPOP-IMZ-1(Figure 21a), iPOP-IMZ-2(Figure 21b), and iPOP-IMZ-3(Figure 21c) in 1 min time intervals when investigated through of UV-vis spectroscopy. As shown in Figures 21d and 21e, the steady decrease in the concentration of the aqueous solution of MnO_4^- with time in the presence of iPOPs and adsorption rate reaches

99.0% for iPOP-IMZ-1, 99.6% for iPOP-IMZ-2 and 99.2% for iPOP-IMZ-3 within four minutes in each case. However, in this analysis, the adsorption process was found to follow the pseudo-second-order kinetics with R^2 value 0.99 for iPOP-IMZ-1, 0.99 for iPOP-IMZ-2, and 0.99 for iPOP-IMZ-3 (Figure 21f).

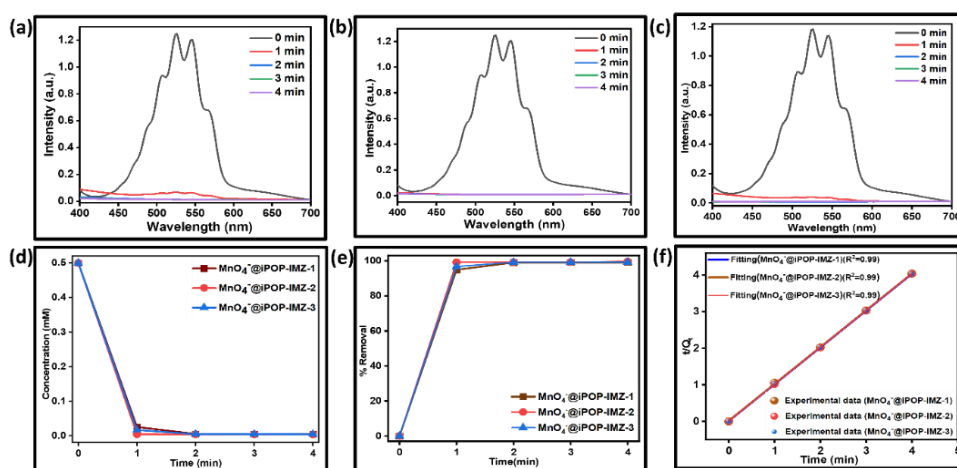


Figure 4.21 The UV-vis spectra, at different times for aqueous solution of MnO_4^- in the presence of (a) iPOP-IMZ-1, (b) iPOP-IMZ-2, (c) iPOP-IMZ-3. (d) Decrease in the concentration and (e) removal (%), with time in the presence of iPOPs (f) The pseudo-second-order kinetics of the aqueous solution of MnO_4^- .

4.5 Analysis of adsorption of anionic dyes by iPOPs

Similarly to metal oxo-anions, multiple organic dyes have also affected the environment, aquatic life, and human health due to their toxic nature. So, here we have also checked the adsorption ability of synthesized materials towards two toxic dyes Methyl Orange (MO). In this analysis also, it has been observed that there is a constant decrement in the characteristic peak (λ_{max}) at 464 nm and 523 nm for the aqueous solution of MO in the presence of polymers iPOP-IMZ-1, iPOP-IMZ-2, and iPOP-IMZ-3 (Figures 22a-22c). In respectable time intervals when investigated through UV-vis spectroscopy. As shown in Figure 22d, the steady decrease in the

concentration of the aqueous solution of MO and Amaranth with time in the presence of iPOPs and adsorption rate reaches 99.13% for iPOP-IMZ-1, 99.46% for iPOP-IMZ-2 and 98.97% and for iPOP-IMZ-3 in MO (Figure 22e). , In this analysis, the adsorption process was found to follow the pseudo-second-order kinetics with R^2 value 0.99 for iPOP-IMZ-1, 0.99 for iPOP-IMZ-2, and 0.99 for iPOP-IMZ-3 (Figure 22f).

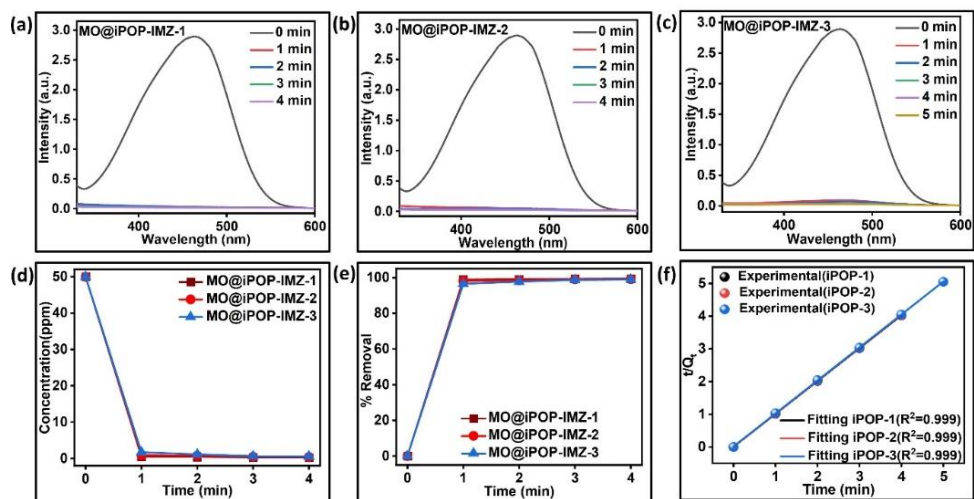


Figure 4.22 The UV-vis spectra, at different times for aqueous solution of Methyl Orange (MO) in the presence of (a) iPOP-IMZ-1, (b) iPOP-IMZ-2, (c) iPOP-IMZ-3. (d) Decrease in the concentration and (e) removal (%), with time in the presence of iPOPs (f) The pseudo-second-order kinetics of the aqueous solution of Methyl Orange (MO).

Similarly to Methyl Orange, Amaranth is also a toxic dye, so we have also checked the adsorption ability of synthesized materials towards two toxic dyes. In this analysis also, it has been observed that there is a constant decrement in the characteristic peak (λ_{max}) at 523 nm for the aqueous solution of Amaranth in the presence of polymers iPOP-IMZ-1, iPOP-IMZ-2, and iPOP-IMZ-3 (Figure 23a-23c) in respective time intervals when investigated through UV-vis spectroscopy. As shown in Figure 23d, the steady decrease in the concentration of the aqueous solution of Amaranth with time in the presence of iPOPs and adsorption rate reaches 99.24% for

iPOP-IMZ-1, 99.4% for iPOP-IMZ-2 and 99.01% for iPOP-IMZ-3 in Amaranth (Figure 23e) adsorption experiment. Also, In this analysis, the adsorption process was found to follow the pseudo-second-order kinetics with R^2 value 0.99 for iPOP-IMZ-1, 0.99 for iPOP-IMZ-2, and 0.98 for iPOP-IMZ-3 (Figure 23f).

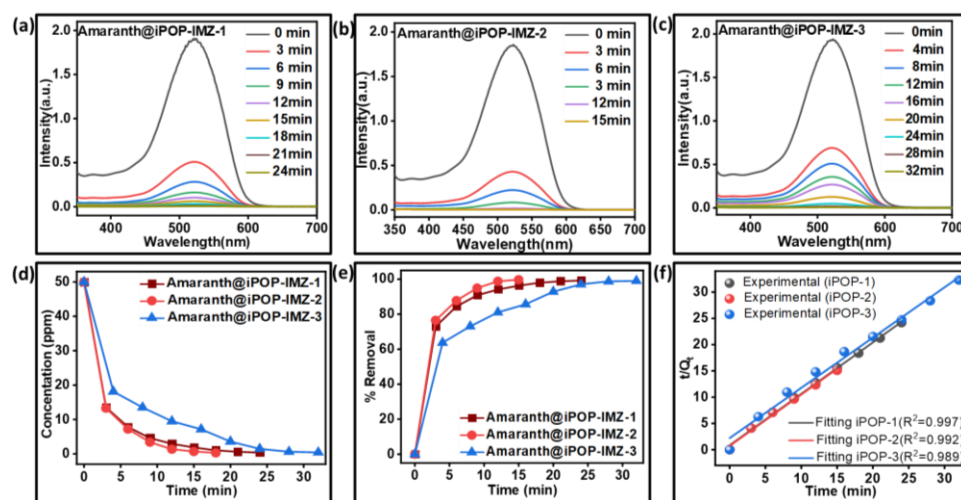


Figure 4.23 The UV-vis spectra, at different times for aqueous solution of Amaranth in the presence of (a) iPOP-IMZ-1, (b) iPOP-IMZ-2, (c) iPOP-IMZ-3. (d) Decrease in the concentration and (e) removal (%), with time in the presence of iPOPs (f) The pseudo-second-order kinetics of the aqueous solution of Amaranth.

The maximum adsorption capacity of iPOPs was calculated towards metal-based oxo anions ($\text{Cr}_2\text{O}_7^{2-}$ and MnO_4^-) and anionic dyes (MO and Amaranth) through the following Langmuir isotherm. The maximum capacities iPOPs towards metal-based oxo anions have come to 519.38 mgg^{-1} , 588.03 mgg^{-1} , 472.28 mgg^{-1} (Figure 24a-24c for $\text{Cr}_2\text{O}_7^{2-}$) and 1218.70 mgg^{-1} , 2031.27 mgg^{-1} , 1213.98 mgg^{-1} (Figure 24d-24f for MnO_4^-) in case of iPOP-IMZ-1, iPOP-IMZ-2 and iPOP-IMZ-3 respectively.

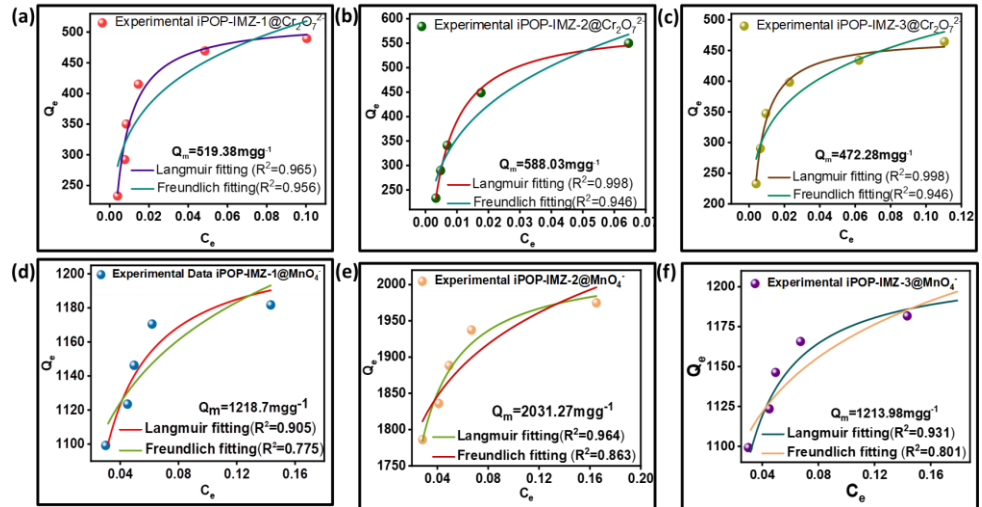


Figure 4.24 Langmuir isotherm of $\text{Cr}_2\text{O}_7^{2-}$ (24a- 24c) and MnO_4^- (24d-24f) in the presence of iPOP-IMZ-1, iPOP-IMZ-2, and iPOP-IMZ-3 respectively

Similarly, the maximum capacities iPOPs towards anionic dyes have come to 763.51 mgg^{-1} , 829.58 mgg^{-1} , and 630.28 mgg^{-1} (Figure 25a-25c for MO) and 260.50 mgg^{-1} , 294.39 mgg^{-1} and 250.39 mgg^{-1} (Figure 24d-24f for Amaranth) in case of iPOP-IMZ-1, iPOP-IMZ-2 and iPOP-IMZ-3, respectively.

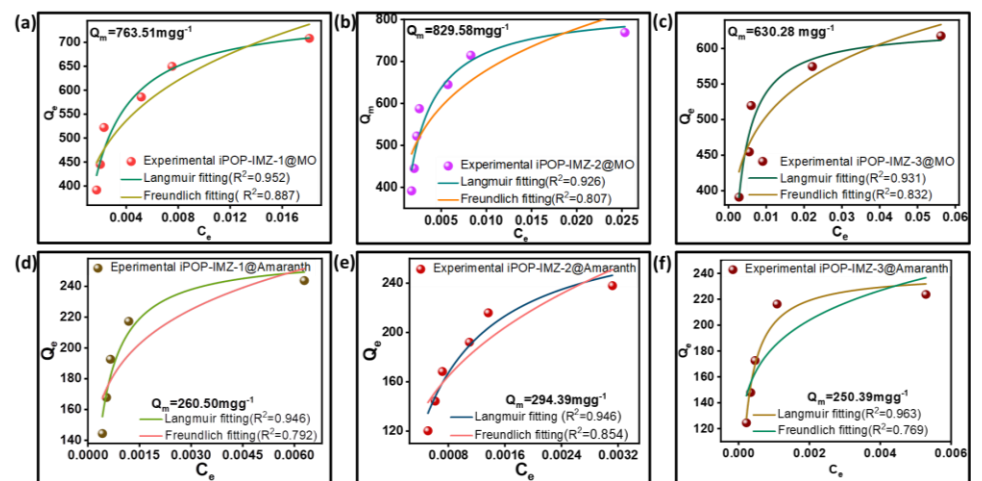


Figure 4.25 Langmuir isotherm of MO (25a- 25c) and Amaranth (25d-25f) in the presence of iPOP-IMZ-1, iPOP-IMZ-2, and iPOP-IMZ-3 respectively

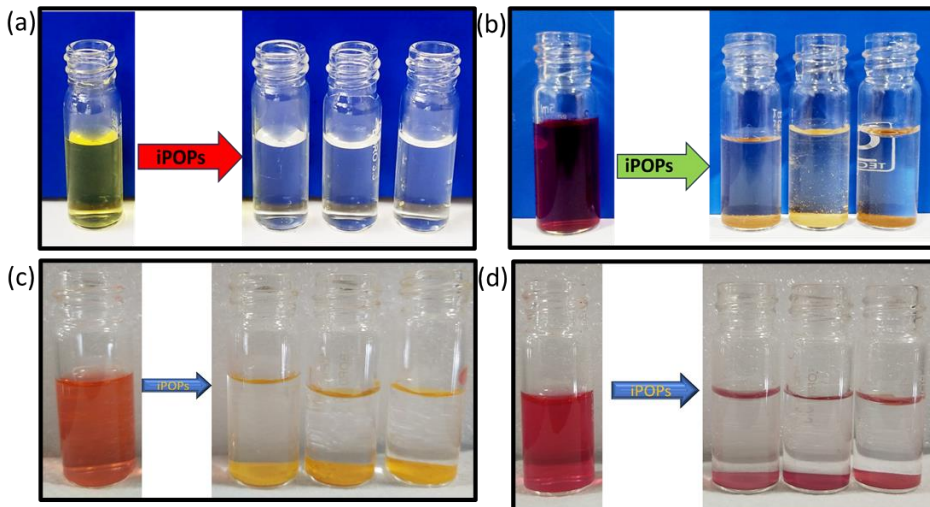


Figure 4.26 Diminish the color of (a) $\text{Cr}_2\text{O}_7^{2-}$, (b) MnO_4^- , (c) MO , and (d) Amaranth in the presence of *iPOPs* respectively

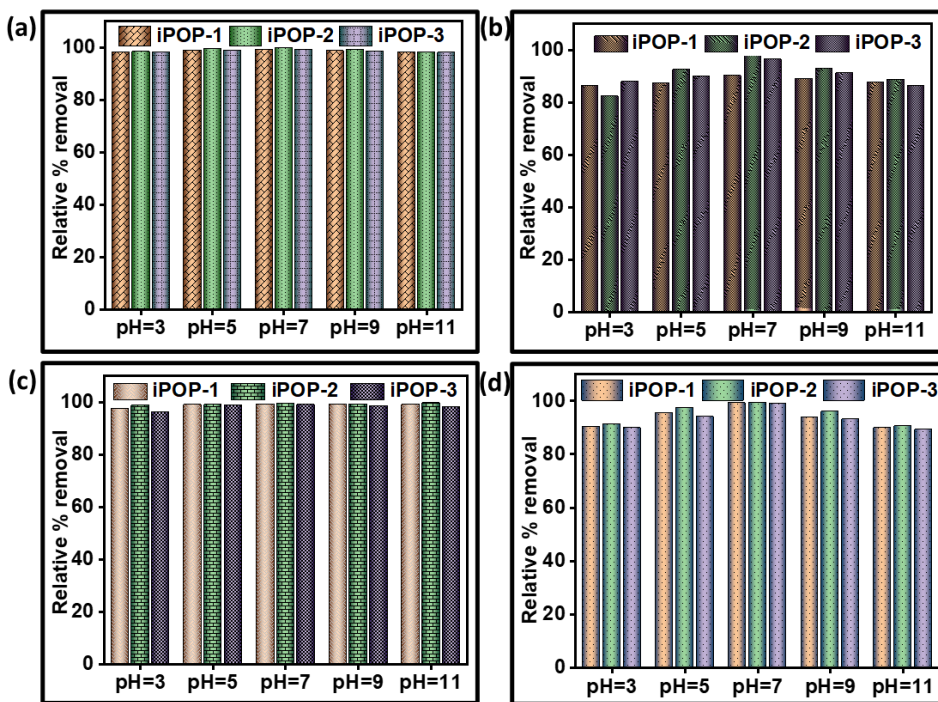


Figure 4.27 Relative % removal at different pH of (a) $\text{Cr}_2\text{O}_7^{2-}$, (b) MnO_4^- , (c) MO , and (d) Amaranth in the presence of *iPOPs* respectively

4.6 Fluorescence sensing

During the investigation of the fluorescence properties of synthesized polymers, it was observed that the fluorescence intensity of polymers has been quenched in the presence of $\text{Cr}_2\text{O}_7^{2-}$ and MnO_4^- . There was a gradual decrease in the fluorescence intensity of iPOPs when adding iPOPs in freshly prepared aqueous solutions of different concentrations (10-100 ppm) of both $\text{Cr}_2\text{O}_7^{2-}$ and MnO_4^- . At the 100 ppm concentration, the fluorescence intensity of iPOP-IMZ-2 was quenched to 82.4 % and 90.0 % in the presence of $\text{Cr}_2\text{O}_7^{2-}$ and MnO_4^- , respectively while the fluorescence intensity of iPOP-IMZ-3 was quenched to 87.2 % and 92.2 % in the presence of $\text{Cr}_2\text{O}_7^{2-}$ and MnO_4^- respectively. In the case of iPOP-IMZ-2, the Stern-Volmer equation ($I_0/I = 1 + K_{sv}C$) was fitted with values of R^2 and obtained K_{sv} is 0.99 and $1.48 \times 10^4 \text{ M}^{-1}$ for detection of $\text{Cr}_2\text{O}_7^{2-}$ (figure 4.28b) and 0.98 and $2.17 \times 10^4 \text{ M}^{-1}$ for detection of MnO_4^- (figure 4.28d) respectively. In the case of iPOP-IMZ-3, the Stern-Volmer equation ($I_0/I = 1 + K_{sv}C$) was fitted with values of R^2 and obtained K_{sv} 0.99 and $6.35 \times 10^4 \text{ M}^{-1}$ for the detection of $\text{Cr}_2\text{O}_7^{2-}$ (figure 4.29b) and 0.98 and $2.03 \times 10^4 \text{ M}^{-1}$ for the detection of MnO_4^- (figure 4.29d) respectively. The obtained LOD is, $2.54 \times 10^{-2} \text{ M}$ and $3.58 \times 10^{-2} \text{ M}$ towards $\text{Cr}_2\text{O}_7^{2-}$ and MnO_4^- respectively by using iPOP-IMZ-2 and $5.93 \times 10^{-2} \text{ M}$ and $3.81 \times 10^{-2} \text{ M}$ towards $\text{Cr}_2\text{O}_7^{2-}$ and MnO_4^- respectively by using iPOP-IMZ-3. The LOD was calculated by using an equation.

$$\frac{3\sigma}{K_{sv}}$$

Where σ is represents the standard deviation of λ_{max} of iPOPs.

The fluorescence behaviors of both fluorescent iPOPs were checked in the presence of different ions (Figure 30).

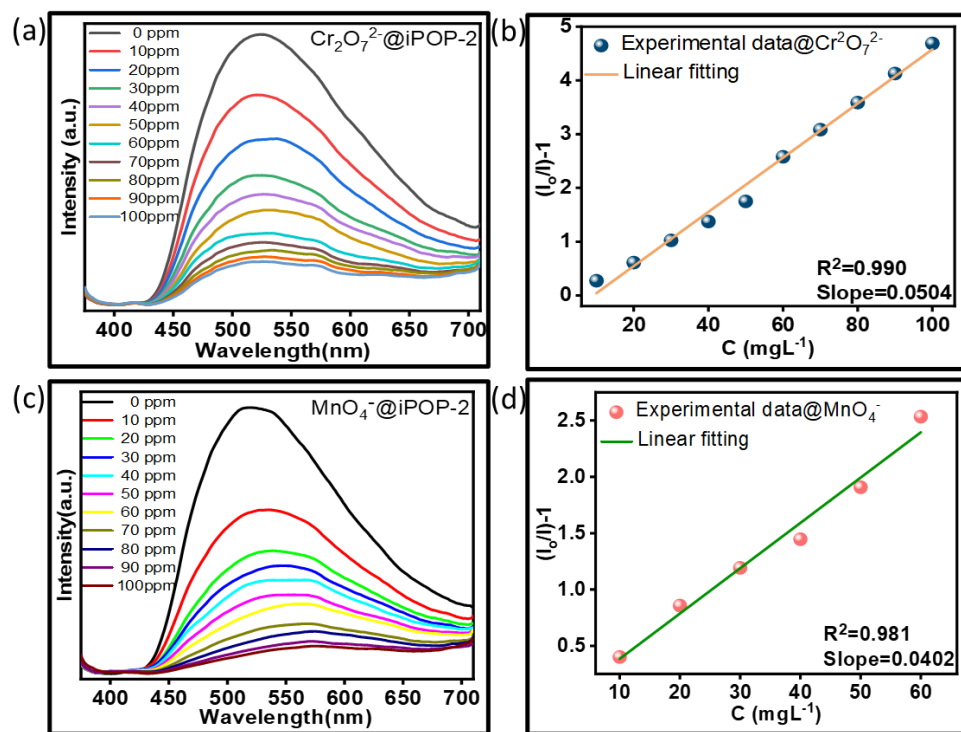


Figure 4.28 In the presence of $\text{Cr}_2\text{O}_7^{2-}$, (a) fluorescence spectra (b) Stern–Volmer equation fitting. In the presence of permanganate ions, (c) fluorescence spectra and (d) Stern–Volmer equation fitting of iPOP-IMZ-2 .

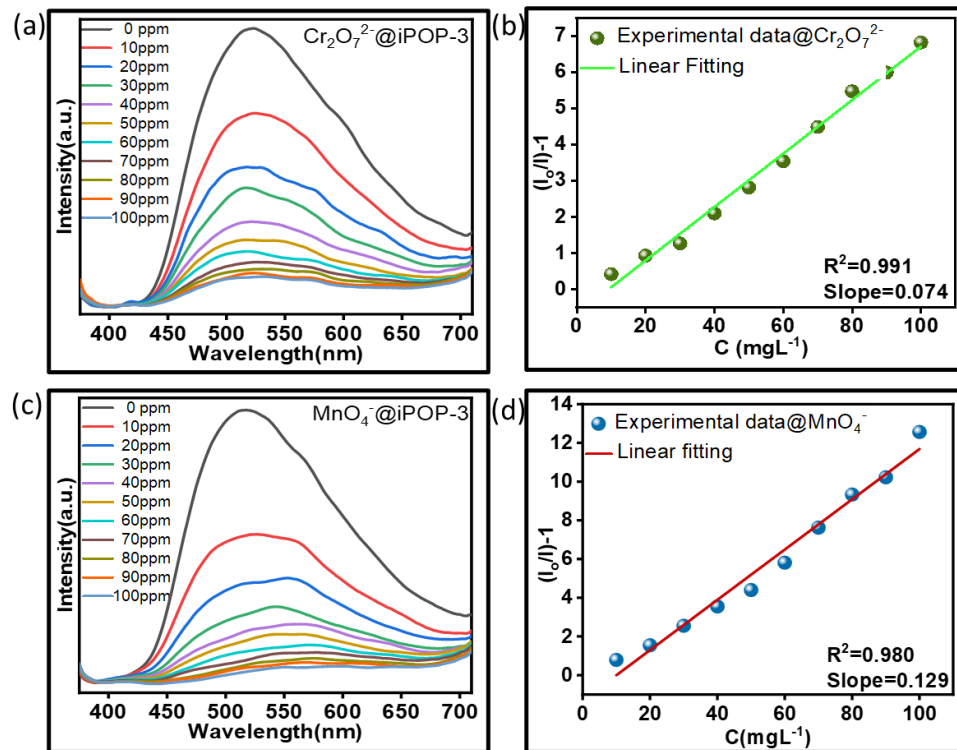


Figure 4.29 In the presence of dichromate ions, (a) fluorescence spectra (b) Stern–Volmer equation fitting. In the presence of permanent ions, (c) fluorescence spectra and (d) Stern–Volmer equation fitting of iPOP-IMZ-3.

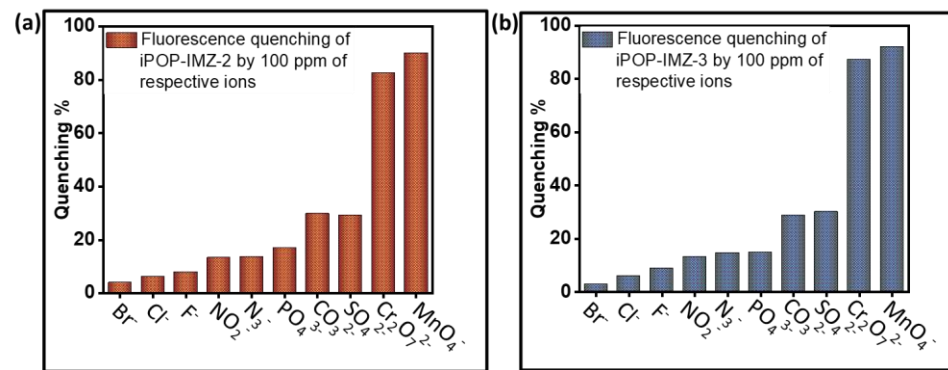
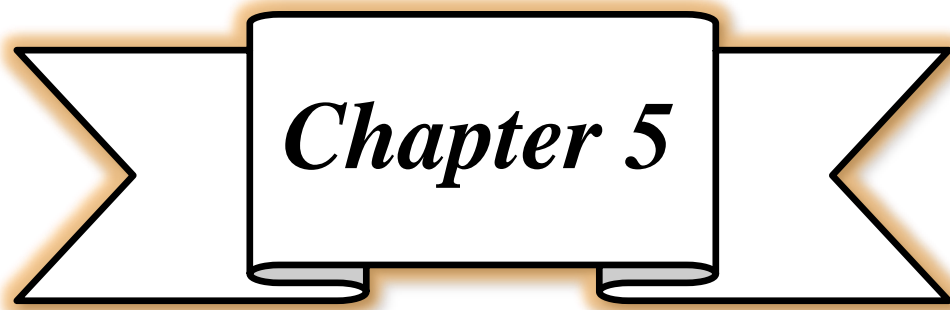


Figure 4.30 Fluorescence quenching of (a) iPOP-IMZ-2 and (b) iPOP-IMZ-3 in the presence of other anions.



Chapter 5

Conclusion & Future scope

5.1 Conclusion

Herein, three imidazolium functionalized ionic porous organic polymers, iPOP-IMZ-1, iPOP-IMZ-2, and iPOP-IMZ-3, are designed and synthesized successfully. They are characterized by FTIR, solid-state ^{13}C NMR, and the thermal stability of iPOPs, which has been investigated by thermal geometric analysis (TGA). The amorphous nature of iPOPs is confirmed through the PXRD pattern. FESEM conducted a morphological investigation of iPOPs. It has been observed that by decreasing the distance between two adjacent cationic centers and increasing the number of cationic centers the polymer network can be optimized for maximum efficiency in the removal of anionic pollutants ($\text{Cr}_2\text{O}_7^{2-}$, MnO_4^- , MO, and Amaranth). It was found that if porous organic polymers have less distance between the cationic centers on their skeleton or have a higher density of cationic centers on the polymeric network, then those polymers show higher adsorption capacity and fast kinetics in the removal of anionic pollutants like synthesized porous organic polymer iPOP-IMZ-2. Due to their luminescent properties, the $\text{Cr}_2\text{O}_7^{2-}$ and MnO_4^- get detected by iPOP-IMZ-2 and iPOP-IMZ-3.

5.2 Future Scope

The synthesized ionic porous organic polymers showed excellent adsorption activity towards ionic pollutants ($\text{Cr}_2\text{O}_7^{2-}$, MnO_4^- , Methyl Orange (MO), and Amaranth), thus it is planned to use these polymers to adsorb Arsenate oxo anions, ionic pesticides, and ionic pharmaceutical drugs, etc. Additionally, considering the antibacterial properties of guanidium-based salts, the antibacterial properties of the synthesized polymers will be further explored.

REFERENCES

- 1 Singer, S.F., 1970. Global effects of environmental pollution. *Eos, Transactions American Geophysical Union*, 51(5), pp.476-478.
- 2 Khan, M.Z., Abbas, D., Ghalib, S.A., Yasmeen, R., Siddiqui, S., Mehmood, N., Zehra, A., Begum, A., Jabeen, T., Yasmeen, G. and Latif, T.A., 2012. Effects of environmental pollution on aquatic vertebrates and inventories of Haleji and Keenjhar Lakes: Ramsar Sites. *Canadian Journal of Pure and Applied Sciences*, 6(1), pp.1759-1783
- 3 Noyes, P.D. and Lema, S.C., 2015. Forecasting the impacts of chemical pollution and climate change interactions on the health of wildlife. *Current Zoology*, 61(4), pp.669-689.
- 4 Keith, L. and Telliard, W., 1979. ES&T special report: priority pollutants: Ia perspective view. *Environmental science & technology*, 13(4), pp.416-423
- 5 Sanchís, J., Kantiani, L., Llorca, M., Rubio, F., Ginebreda, A., Fraile, J., Garrido, T. and Farré, M., 2012. Determination of glyphosate in groundwater samples using an ultrasensitive immunoassay and confirmation by on-line solid-phase extraction followed by liquid chromatography coupled to tandem mass spectrometry. *Analytical and Bioanalytical Chemistry*, 402, pp.2335-2345.
- 6 Mishima, A., 1992. *Bitter sea: the human cost of minamata disease*. Tuttle Publishing.
- 7 Verma, R. and Dwivedi, P., 2013. Heavy metal water pollution-A case study. *Recent Research in Science and Technology*, 5(5).

- 8 Zeitoun, M.M. and Mehana, E.E., 2014. Impact of water pollution with heavy metals on fish health: overview and updates. *Global Veterinaria*, 12(2), pp.219-231.
- 9 Tkaczyk, A., Mitrowska, K. and Posyniak, A., 2020. Synthetic organic dyes as contaminants of the aquatic environment and their implications for ecosystems: A review. *Science of the total environment*, 717, p.137222.
- 10 Anliker, R., Butler, G.C., Clarke, E.A., Förstner, U., Funke, W., Hyslop, C., Kaiser, G., Rappe, C., Russow, J., Tölg, G. and Zander, M., 1980. Organic dyes and pigments. *Anthropogenic compounds*, pp.181-215.
- 11 Barnhart, J., 1997. Occurrences, uses, and properties of chromium. *Regulatory toxicology and pharmacology*, 26(1), pp.S3-S7.
- 12 Rahman, Z., Thomas, L., Chetri, S.P., Bodhankar, S., Kumar, V. and Naidu, R., 2023. A comprehensive review on chromium (Cr) contamination and Cr (VI)-resistant extremophiles in diverse extreme environments. *Environmental Science and Pollution Research*, 30(21), pp.59163-59193.
- 13 Anliker, R., Butler, G.C., Clarke, E.A., Förstner, U., Funke, W., Hyslop, C., Kaiser, G., Rappe, C., Russow, J., Tölg, G. and Zander, M., 1980. Organic dyes and pigments. *Anthropogenic compounds*, pp.181-215.
- 14 Lewicki, S., Zdanowski, R., Krzyzowska, M., Lewicka, A., Debski, B., Niemcewicz, M. and Goniewicz, M., 2014. The role of Chromium III in the organism and its possible use in diabetes and obesity treatment. *Annals of Agricultural and Environmental Medicine*, 21(2).

- 15 Gupta, A., Mumtaz, S., Li, C.H., Hussain, I. and Rotello, V.M., 2019. Combatting antibiotic-resistant bacteria using nanomaterials. *Chemical Society Reviews*, 48(2), pp.415-427.
- 16 Tumolo, M., Ancona, V., De Paola, D., Losacco, D., Campanale, C., Massarelli, C. and Uricchio, V.F., 2020. Chromium pollution in European water, sources, health risk, and remediation strategies: An overview. *International journal of environmental research and public health*, 17(15), p.5438.
- 17 Stambulska, Uliana Ya, Maria M. Bayliak, and Volodymyr I. Lushchak. "Chromium (VI) toxicity in legume plants: modulation effects of rhizobial symbiosis." *BioMed research international* 2018 (2018).
- 18 Prasad, S., Yadav, K.K., Kumar, S., Gupta, N., Cabral-Pinto, M.M., Rezania, S., Radwan, N. and Alam, J., 2021. Chromium contamination and effect on environmental health and its remediation: A sustainable approaches. *Journal of Environmental Management*, 285, p.112174.
- 19 Dickson, J.O., Harsh, J.B., Flury, M., Lukens, W.W. and Pierce, E.M., 2014. Competitive incorporation of perrhenate and nitrate into sodalite. *Environmental science & technology*, 48(21), pp.12851-12857.
- 20 Meisinger, Q.C., Stahl, C.M., Andre, M.P., Kinney, T.B. and Newton, I.G., 2016. Radiation protection for the fluoroscopy operator and staff. *American Journal of Roentgenology*, 207(4), pp.745-754.
- 21 Banerjee, D., Kim, D., Schweiger, M.J., Kruger, A.A. and Thallapally, P.K., 2016. Removal of TcO⁴⁻ ions from solution:

- materials and future outlook. *Chemical Society Reviews*, 45(10), pp.2724-2739.
- 22 Tkaczyk, A., Mitrowska, K. and Posyniak, A., 2020. Synthetic organic dyes as contaminants of the aquatic environment and their implications for ecosystems: A review. *Science of the total environment*, 717, p.137222.
- 23 Islam, T., Repon, M.R., Islam, T., Sarwar, Z. and Rahman, M.M., 2023. Impact of textile dyes on health and ecosystem: A review of structure, causes, and potential solutions. *Environmental Science and Pollution Research*, 30(4), pp.9207-9242.
- 24 Ismail, M., Akhtar, K., Khan, M.I., Kamal, T., Khan, M.A., M Asiri, A., Seo, J. and Khan, S.B., 2019. Pollution, toxicity and carcinogenicity of organic dyes and their catalytic bio-remediation. *Current pharmaceutical design*, 25(34), pp.3645-3663.
- 25 Nahiun, K.M., Sarker, B., Keya, K.N., Mahir, F.I., Shahida, S. and Khan, R.A., 2021. A review on the methods of industrial waste water treatment. *Scientific Review*, 7(3), pp.20-31.
- 26 Khafaie, M.A., Yajnik, C.S., Salvi, S.S. and Ojha, A., 2016. Critical review of air pollution health effects with special concern on respiratory health. *Journal of air pollution and health*, 1(2), pp.123-136.
- 27 Soni, R., Soni, M. and Shukla, D.P., 2020. Emerging techniques and materials for water pollutants detection. *Sensors in Water Pollutants Monitoring: Role of Material*, pp.277-297.
- 28 Walekar, L., Dutta, T., Kumar, P., Ok, Y.S., Pawar, S., Deep, A. and Kim, K.H., 2017. Functionalized fluorescent nanomaterials for

sensing pollutants in the environment: A critical review. *TrAC Trends in Analytical Chemistry*, 97, pp.458-467.

- 29 Hanafi, M.F. and Sapawe, N., 2020. A review on the current techniques and technologies of organic pollutants removal from water/wastewater. *Materials Today: Proceedings*, 31, pp.A158-A165.
- 30 El-Baz, A.A.A., Hendy, I.A., Dohdoh, A.M. and Srour, M.I., 2020. Adsorption technique for pollutants removal; current new trends and future challenges—A Review. *The Egyptian International Journal of Engineering Sciences and Technology*, 32(Civil and Architectural Engineering), pp.1-24.
- 31 Cevallos-Mendoza, J., Amorim, C.G., Rodríguez-Díaz, J.M. and Montenegro, M.D.C.B., 2022. Removal of contaminants from water by membrane filtration: a review. *Membranes*, 12(6), p.570.
- 32 Md Anwar, H. and Chowdhury, R., 2020. Remediation of polluted river water by biological, chemical, ecological and engineering processes. *Sustainability*, 12(17), p.7017.
- 33 Osman, A.I., Elgarahy, A.M., Eltaweil, A.S., Abd El-Monaem, E.M., El-Aqapa, H.G., Park, Y., Hwang, Y., Ayati, A., Farghali, M., Ihara, I. and Al-Muhtaseb, A.A.H., 2023. Biofuel production, hydrogen production and water remediation by photocatalysis, biocatalysis and electrocatalysis. *Environmental Chemistry Letters*, 21(3), pp.1315-1379.
- 35 Rashid, R., Shafiq, I., Akhter, P., Iqbal, M.J. and Hussain, M., 2021. A state-of-the-art review on wastewater treatment techniques: the effectiveness of adsorption method. *Environmental Science and Pollution Research*, 28, pp.9050-9066.

- 36 Muharrem, I.N.C.E. and Ince, O.K., 2017. An overview of adsorption technique for heavy metal removal from water/wastewater: a critical review. *International Journal of Pure and Applied Sciences*, 3(2), pp.10-19.
- 37 Sun, Q., Aguila, B., Song, Y. and Ma, S., 2020. Tailored porous organic polymers for task-specific water purification. *Accounts of chemical research*, 53(4), pp.812-821.
- 38 Modak, A., Bhanja, P., Selvaraj, M. and Bhaumik, A., 2020. Functionalized porous organic materials as efficient media for the adsorptive removal of Hg (II) ions. *Environmental Science: Nano*, 7(10), pp.2887-2923.
- 39 Wang, S., Li, H., Huang, H., Cao, X., Chen, X. and Cao, D., 2022. Porous organic polymers as a platform for sensing applications. *Chemical Society Reviews*, 51(6), pp.2031-2080.
- 40 Li, Z. and Yang, Y.W., 2022. Macrocyclic-based porous organic polymers for separation, sensing, and catalysis. *Advanced Materials*, 34(6), p.2107401.
- 41 Wang, S., Li, H., Huang, H., Cao, X., Chen, X. and Cao, D., 2022. Porous organic polymers as a platform for sensing applications. *Chemical Society Reviews*, 51(6), pp.2031-2080.
- 42 Mohamed, M.G., EL-Mahdy, A.F., Kotp, M.G. and Kuo, S.W., 2022. Advances in porous organic polymers: Syntheses, structures, and diverse applications. *Materials Advances*, 3(2), pp.707-733.
- 43 Lu, W., Wei, Z., Yuan, D., Tian, J., Fordham, S. and Zhou, H.C., 2014. Rational design and synthesis of porous polymer networks: toward high surface area. *Chemistry of Materials*, 26(15), pp.4589-4597.

- 44 M. G. Mohamed, S. M. Ebrahium, A. S. Hammam, S. W. Kuo and K. I. Aly, Enhanced CO₂ capture in nitrogen-enriched microporous carbons derived from Polybenzoxazines containing azobenzene and carboxylic acid units, *J. Polym. Res.*, 2020, 27, 197
- 45 Z. Qian, Z. J. Wang and K. A. I. Zhang, Covalent Triazine Frameworks as Emerging Heterogeneous Photocatalysts, *Chem. Mater.*, 2021, 33, 1909–1926
- 46 Mohamed, M.G., EL-Mahdy, A.F., Kotp, M.G. and Kuo, S.W., 2022. Advances in porous organic polymers: Syntheses, structures, and diverse applications. *Materials Advances*, 3(2), pp.707-733
- 47 A. Schneemann, R. Dong, F. Schwotzer, H. Zhong, I. Senkovska, X. Feng and S. Kaskel, 2D framework materials for energy applications, *Chem. Sci.*, 2021, 12, 1600–1619
- 48 V. Singh and H. R. Byon, Advances in electrochemical energy storage with covalent organic frameworks, *Mater. Adv.*, 2021, 2, 3188–3212
- 49 H. Vardhan, A. Nafady, A. M. Al-Enizi and S. Ma, Pore surface engineering of covalent organic frameworks: structural diversity and applications, *Nanoscale*, 2019, 11, 21679–21708
- 50 X. Zhao, P. Pachfule and A. Thomas, Covalent organic frameworks (COFs) for electrochemical applications, *Chem. Soc. Rev.*, 2021, 50, 6871–6913
- 51 M. S. Lohse and T. Bein, Covalent Organic Frameworks: Structures, Synthesis, and Applications, *Adv. Funct. Mater.*, 2018, 28, 1705553
- 52 J. Huang and S. Richard Turner, Hypercrosslinked Polymers: A Review, *Polym. Rev.*, 2018, 58, 1–41
- 53 Z. Wei, Q. Chen and H. Liu, Hydroxyl modified hypercrosslinked polymers: targeting high efficient adsorption separation towards aniline, *New J. Chem.*, 2021, 45, 11607–11617

- 54 M. Errahali, G. Gatti, L. Tei, G. Paul, G. Rolla, L. Canti, A. Fraccarollo, M. Cossi, A. Comotti, P. Sozzani and L. Marchese, Microporous Hyper-crosslinked Aromatic Polymers Designed for Methane and Carbon Dioxide Adsorption, *J. Phys. Chem. C*, 2014, 118, 28699–28710
- 55 S. Luo, Z. Zeng, H. Wang, W. Xiong, B. Song, C. Zhou, A. Duan, X. Tan, Q. He, G. Zeng, Z. Liu and R. Xiao, Recent progress in conjugated microporous polymers for clean energy: Synthesis, modification, computer simulations, and applications, *Prog. Polym. Sci.*, 2021, 115, 101374
- 56 X. Sheng, H. Shi, L. Yanga, P. Shao, K. Yu and X. Luo, Rationally designed conjugated microporous polymers for contaminants adsorption, *Sci. Total Environ.*, 2021, 750, 141683
- 57 Y. He, Z. Cheng, H. Zuo, C. Yan and Y. Liao, Green synthesis of pyridyl conjugated microporous polymers as precursors for porous carbon microspheres for efficient electrochemical energy storage, *ChemElectroChem*, 2020, 7, 959–966
- 58 Mohamed, M.G., EL-Mahdy, A.F., Kotp, M.G. and Kuo, S.W., 2022. Advances in porous organic polymers: Syntheses, structures, and diverse applications. *Materials Advances*, 3(2), pp.707-733.
- 59 Chakraborty, A., Sarkar, S., Nag, P., Ranjan, R., Vennapusa, S.R. and Mukhopadhyay, S., 2023. Exploring multifunctional applications of a luminescent covalent triazine polymer in acid vapour sensing, CO₂ capture, dye removal, and turn-off fluorescence sensing of dichromate ions. *Materials Chemistry Frontiers*, 7(9), pp.1831-1840.
- 60 Sarkar, S., Ghosh, T., Chakraborty, A., Majhi, J., Nag, P., Bandyopadhyay, A., Vennapusa, S.R., Kumar, R. and Mukhopadhyay, S., 2023. Exploring a Redox-Active Ionic Porous Organic Polymer in Environmental Remediation and Electrochromic Application. *ACS Applied Materials & Interfaces*

- 61 Zhao, W., Zhang, F., Yang, L., Bi, S., Wu, D., Yao, Y., Wagner, M., Graf, R., Hansen, M.R., Zhuang, X. and Feng, X., 2016. Anionic porous polymers with tunable structures and catalytic properties. *Journal of materials chemistry A*, 4(39), pp.15162-15168
- 62 Xu, J., Xu, J., Moon, H., Sintim, H.O. and Lee, H., 2020. Zwitterionic porous conjugated polymers as a versatile platform for antibiofouling implantable bioelectronics. *ACS applied polymer materials*, 2(2), pp.528-536.
- 63 Zhang, C., Li, G. and Zhang, Z., 2015. A hydrazone covalent organic polymer based micro-solid phase extraction for online analysis of trace Sudan dyes in food samples. *Journal of Chromatography A*, 1419, pp.1-9.
- 64 Sarkar, S., Chakraborty, A., Ranjan, R., Nag, P., Vennapusa, S.R. and Mukhopadhyay, S., 2022. A bifunctional imidazolium-functionalized ionic porous organic polymer in water remediation. *Materials Chemistry Frontiers*, 6(20), pp.3070-3083
- 65 Patra, B.C., Khilari, S., Satyanarayana, L., Pradhan, D. and Bhaumik, A., 2016. A new benzimidazole based covalent organic polymer having high energy storage capacity. *Chemical communications*, 52(48), pp.7592-7595.
- 66 Stegbauer, L., Hahn, M.W., Jentys, A., Savasci, G., Ochsenfeld, C., Lercher, J.A. and Lotsch, B.V., 2015. Tunable water and CO₂ sorption properties in isostructural azine-based covalent organic frameworks through polarity engineering. *Chemistry of Materials*, 27(23), pp.7874-7881.
- 67 54 Cote, A.P., Benin, A.I., Ockwig, N.W., O'Keeffe, M., Matzger, A.J. and Yaghi, O.M., 2005. Porous, crystalline, covalent organic frameworks. *science*, 310(5751), pp.1166-1170.
- 68 55 Wan, S., Gándara, F., Asano, A., Furukawa, H., Saeki, A., Dey, S.K., Liao, L., Ambrogio, M.W., Botros, Y.Y., Duan, X. and Seki,

- S., 2011. Covalent organic frameworks with high charge carrier mobility. *Chemistry of Materials*, 23(18), pp.4094-4097.
- 69 De Paul, S.M., Zwanziger, J.W., Ulrich, R., Wiesner, U. and Spiess, H.W., 1999. Structure, Mobility, and Interface Characterization of Self-Organized Organic– Inorganic Hybrid Materials by Solid-State NMR. *Journal of the American Chemical Society*, 121(24), pp.5727-5736.
- 70 Feng, L., Zhang, S., Sun, X., Dong, A. and Chen, Q., 2018. Boronic acid-functionalized porous polycarbazoles: preparation, adsorption performance, and heterogeneous catalysts for selective oxidation. *Journal of materials science*, 53, pp.15025-1503
- 71 Xu, Y., Chang, D., Feng, S., Zhang, C. and Jiang, J.X., 2016. BODIPY-containing porous organic polymers for gas adsorption. *New Journal of Chemistry*, 40(11), pp.9415-9423.
- 72 Briggs, M.E. and Cooper, A.I., 2017. A perspective on the synthesis, purification, and characterization of porous organic cages. *Chemistry of Materials*, 29(1), pp.149-157.
- 73 Mohammed, A. and Abdullah, A., 2018, November. Scanning electron microscopy (SEM): A review. In *Proceedings of the 2018 International Conference on Hydraulics and Pneumatics HERVEX, Băile Govora, Romania (Vol. 2018, pp. 7-9)*.
- 74 Zhang, P., Wang, Z., Cheng, P., Chen, Y. and Zhang, Z., 2021. Design and application of ionic covalent organic frameworks. *Coordination Chemistry Reviews*, 438, p.213873.
- 75 Ma, H., Liu, B., Li, B., Zhang, L., Li, Y.G., Tan, H.Q., Zang, H.Y. and Zhu, G., 2016. Cationic covalent organic frameworks: a simple platform of anionic exchange for porosity tuning and proton

- conduction. *Journal of the American Chemical Society*, 138(18), pp.5897-5903.
- 76 Jiao, S., Deng, L., Zhang, X., Zhang, Y., Liu, K., Li, S., Wang, L. and Ma, D., 2021. Evaluation of an ionic porous organic polymer for water remediation. *ACS Applied Materials & Interfaces*, 13(33), pp.39404-39413.
- 77 Liu, Z.W. and Han, B.H., 2019. Evaluation of an imidazolium-based porous organic polymer as radioactive waste scavenger. *Environmental Science & Technology*, 54(1), pp.216-224.
- 78 Chandra, S., Hassan, A., Prince, Alam, A. and Das, N., 2022. Rapid and efficient removal of diverse anionic water contaminants using a guanidium-based ionic covalent organic network (iCON). *ACS Applied Polymer Materials*, 4(9), pp.6630-6641.
- 79 Jansone-Popova, S., Moinel, A., Schott, J.A., Mahurin, S.M., Popovs, I., Veith, G.M. and Moyer, B.A., 2018. Guanidinium-based ionic covalent organic framework for rapid and selective removal of toxic Cr (VI) oxoanions from water. *Environmental science & technology*, 53(2), pp.878-883.
- 80 Westerhoff, P.; Zimmerman, J. B.; Field, J.; Lowry, G. Making Waves. *Environ. Sci. Technol.* 2020, 54, 6449–6450.
- 81 C. Zamora-Ledezma, D. Negrete-Bolagay, F. Figueroa, E. Zamora-Ledezma, M. Ni, F. Alexis and V. H. Guerrero, Heavy Metal Water Pollution: A Fresh Look about Hazards, Novel and Conventional Remediation Methods, *Environ. Technol. Innovation*, 2021, 22, 101504.
- 82 R. von Burg and D. Liu, Chromium and Hexavalent Chromium, *J. Appl. Toxicol.*, 1993, 13, 225–230.

83 Bilal, M., Mehmood, S. and Iqbal, H.M., 2020. The beast of beauty: environmental and health concerns of toxic components in cosmetics. *Cosmetics*, 7(1), p.13.

